

# Numerical evaluation of slepton pair production

*Using VegasFlow and PDFFlow to speed up the calculation of cross sections for slepton and sneutrino pair production at the LHC*

Martin Moen Carstensen



Thesis submitted for the degree of  
Master in Theoretical Physics  
60 credits

Department of physics  
Faculty of mathematics and natural sciences

UNIVERSITY OF OSLO

Spring 2022



# Numerical evaluation of slepton pair production

*Using VegasFlow and PDFFlow to speed up the calculation of cross sections for slepton and sneutrino pair production at the LHC*

Martin Moen Carstensen

© 2022 Martin Moen Carstensen

Numerical evaluation of slepton pair production

<http://www.duo.uio.no/>

Printed: Reprosentralen, University of Oslo

# Abstract

In the search for new physics beyond the standard model, much of the computational time is spent calculating the same cross section numerous times. Especially for collisions involving protons, the evaluations of parton distribution functions are computationally demanding. In this thesis we focus on slepton pair production and the evaluation of the parton distribution functions by first calculating the hard partonic cross section to leading order using relevant Feynman rules from the standard model and the minimal supersymmetric standard model. This is done by first developing the Feynman rules of Abelian and non-Abelian gauge theories through the use of group theory and path integrals. This leads us to construct an invariant  $SU(N)$  Lagrangian and find the corresponding Feynman rules. We also see that the gauge fixing quantization procedure by Faddeev and Popov introduce ghost fields to the theory.

From the general  $SU(N)$  Lagrangian, we can find the Feynman rules for the theory of quantum chromodynamics (QCD) by considering the  $SU(3)$  group. QCD is the theory of quarks and gluons and is used together with the parton model to calculate the deep inelastic scattering result for structure functions and introduce parton distribution functions. We then introduce the minimal supersymmetric standard model to calculate the Drell-Yan  $pp \rightarrow \tilde{l}_i \tilde{l}_j^*$  cross section to leading order while the next-to-leading order results are summarized.

We use the modules `VegasFlow` and `PDFFlow` to numerically evaluate the full cross section and the corresponding uncertainties. Our data can be compared to similar results where we did not take advantage of these modules. Upon doing so, we find a nearly 50% time decrease in evaluation time with the use of the modules. This increased efficiency shows that the inclusion of `VegasFlow` and `PDFFlow` optimizes the evaluation of the parton distribution functions, therefore reducing the amount of time spent calculating the same cross section.

# Sammen drag

I søket etter ny fysikk videre etter standard modellen brukes det mye tid på å regne ut det samme tverrsnittet flere ganger. Spesielt for kollisjoner som involverer protoner så er parton distribusjon funksjonene veldig krevende å regne ut. I denne avhandlingen fokuserer vi på slepton par produksjon og evalueringen av parton distribusjon funksjonene ved å først regne ut tverrsnittet til det ledende order ved å bruke relevante Feynman regler fra standard modellen, og den minimale supersymmetriske standard modellen. Dette blir gjort ved å først utvikle Feynman reglene for Abelske og ikke-Abelske gauge teorier ved å bruke gruppe teori og vei integraler. Dette gjør at vi kan konstruere en invariant  $SU(N)$  Lagrangian og deretter finne de tilsvarende Feynman reglene. Vi ser også at den gauge fiksete kvantiseringens prosedyren til Faddeev og Popov introduserer såkalte spåkelsesfelt til teorien.

Fra den generelle  $SU(N)$  Lagrangianen, så kan vi finne Feynmanreglene til teorien om kvantekromodynamikk ved å ta i betraktning  $SU(3)$  gruppen. Kvantekromodynamikk er teorien som omhandler kvarker og gluoner og den blir brukt sammen med parton modellen til å regne ut resultatet for struktur funksjonene fra dypt inelastisk spredning og til å introdusere parton distribusjons funksjoner. Deretter gir vi et overblikk over den minimale supersymmetriske standard modellen slik at vi kan regne ut Drell-Yan  $pp \rightarrow \tilde{l}_i \tilde{l}_j$  tverrsnittet til ledende orden, mens det nest-ledende orden blir sitert.

Vi bruker modulene **VegasFlow** og **PDFFlow** til å beregne det fulle tverrsnittet numerisk og de tilsvarende usikkerhetene. Vår data kan da sammenlignes med tilsvarende resultater der vi ikke brukte de overnevnte modulene. Fra dette fant vi en forbedring i tidsbruk på nesten 50% i evalueringstiden ved å bruke disse modellene. Denne økningen i effektivitet viser at det å inkludere **VegasFlow** og **PDFFlow** optimerer evalueringen av parton distribusjon funksjonene, og dermed reduserer mengden tid brukt på å regne ut det samme tverrsnittet.



# Acknowledgements

Firstly, a big thank you should be directed to my supervisor, Are Raklev, for supporting me with patience and encouragement as I worked through the subject of this thesis. The detailed feedback have been immensely helpful in the completion of the thesis and I am thankful that you have always taken time out of your schedule to answer any questions I had. Additionally, I would also like to thank the entire cross section group for great discussions that stimulated, and in particular Anders Kvellestad and Lasse Braseth for stimulating conversations.

I would also like to thank the rest of the theory group for making these two years into very memorable experience, with a special thank you to Øyvind Fløvig and Benedicte Nyheim for great support and many good talks in our three person office. For everyone I have met and all the friendships I have made from my five years at the university, I would like to thank you all for all the help, guidance and fantastic memories. There are too many people to mention, but I thank each and everyone of you.

Last but not least, a huge thank you to my girlfriend, Marisa. She has been the rock in my life that I needed, and the love, support and encouragement that I have gotten from her has been vital in order to complete this thesis.





# Contents

<b>Introduction</b>	<b>1</b>
<b>1 Basics of Quantum Field Theory</b>	<b>3</b>
1.1 Group Theory	3
1.1.1 Lie Groups	5
1.1.2 Representations of $SU(N)$	7
1.2 Gauge theory	9
1.2.1 Abelian gauge theory	9
1.2.2 Non-Abelian gauge theory	11
1.3 Quantum Yang-Mills theory	14
1.3.1 Path integral formulation	14
1.3.2 Path integrals for scalar Abelian theory	15
1.3.3 Quantization of non-Abelian theory	17
<b>2 From partons to QCD</b>	<b>20</b>
2.1 Coulomb scattering	20
2.1.1 Deep inelastic Coulomb scattering	22
2.1.2 Parton Model	24
2.1.3 Parton distribution functions	25
2.2 Quantum chromodynamics and DIS	28
2.2.1 QCD from gauge theories	28
2.2.2 Deep inelastic scattering from QCD	31
2.3 Factorization of the PDFs	35
2.3.1 Outline of factorization proof	35
<b>3 Beyond the standard model</b>	<b>39</b>
3.1 Supersymmetry	39
3.2 Slepton pair production at LHC	42
3.2.1 Kinematics of the cross section	42
3.2.2 Calculation of the LO Drell-Yan cross section	44
3.2.3 NLO results for slepton pair production	46

<b>4</b>	<b>Numerical Calculation of Cross Sections</b>	<b>49</b>
4.1	Parton distribution functions . . . . .	49
4.2	Numerical error calculations . . . . .	51
4.2.1	Factorization and renormalization scale error . . . . .	51
4.2.2	PDF uncertainties . . . . .	51
4.2.3	Adding $\alpha_s$ uncertainties . . . . .	52
4.3	Results of numerical calculations . . . . .	53
	<b>Conclusion</b>	<b>60</b>
<b>A</b>	<b>Code repository</b>	<b>62</b>

# Introduction

The standard model is one of the best tested and precise physics models that we have today. It is the theory of the fundamental interaction between elementary particles such as leptons and quarks, and this model includes the weak, strong and electromagnetic interactions between these particles. The standard model has been immensely successful in predicting the behavior of the fundamental particles through extensive experimental testing at different particle colliders such as the Large Hadron Collider (LHC) at CERN or the Tevatron at Fermilab. As the LHC was built to search for evidence of physics beyond the standard model, this collider was engineered to reach new untested energies and to narrow the precision on measurements of different observables such as the masses of particles. The biggest achievement of the standard model was the successful prediction and subsequent discovery of the Higgs boson which was predicted through spontaneous symmetry breaking of the gauge symmetries, which is the fundamental mathematic theory behind the standard model.

At the LHC we collide protons with high energies and in these collisions one parton from each of the colliding protons will interact resulting in the production of other particles such as leptons or hadrons. These new particles then form particle jets that the detectors can measure. To study these collisions here we will focus on the mechanisms at work in the collision of the proton pair and the interacting partons. This is done by starting from the parton model of the protons, which is a model for describing the collisions, and how the constituent particles interact with eachother. This introduces the concept of parton distribution functions which gives a description as to how the momentum of the proton is divided amongst these constituents, such as the up and down quark and the gluons.

With the increase in energy that the LHC can provide, we can use the data from the collider to search for new physics beyond the standard model. One such candidate of beyond the standard model physics is the theory of supersymmetry. This theory predicts that there exist scalar supersymmetric particles such as sleptons and squarks. These particles could be created in proton collisions and it is the production of sleptons, the supersymmetric partners of the ordinary leptons, that will be discussed in this thesis.

A current big bottleneck in the development of high energy particle physics is the computational time it takes to numerically evaluate the interactions containing protons because of the experimentally evaluated parton distribution functions. In addition, with the search for new physics we need to explore a multi-dimensional space of new parameters in order to figure out which models are consistent with the experimental data provided from different experiments. For instance, the Minimal Supersymmetric standard model (MSSM) contains several new parameters such as the masses of the different new particles. These new parameters must be consistent with previous measurements, and should also be able to explain any new inconsistencies between experimental data and the predictions from the standard model. Such testing requires

several repeated evaluations of the same cross section at different points in the parameter space in order to generate enough data to make comparisons.

**Outline of the thesis** This thesis will first give a brief overview on the necessary quantum field theory that is needed in order to analytically and numerically calculate cross sections. We will then present and study different tools and modules such as `VegasFlow` and `PDFFlow` that are used to increase the speed of the calculations. Lastly, we will present the results using these modules and evaluate whether or not we achieved the desired speed up.

Chapter 1 will therefore give a brief overview of Quantum Field Theory, the underlying basis of the entire thesis, and it is here where we will focus on how the theory is built from Lagrangians and gauge theories to the development of the standard model.

Then chapter 2 will include a brief historical angle looking at how physicists figured out how to calculate the famous Deep Inelastic scattering from the parton model to the development of quantum chromodynamics (QCD) and the introduction of parton distribution functions.

In chapter 3 we will introduce supersymmetry and give a motivation as to why we need to be looking at new physics and why the standard model will not be the final model of physics. This will then lead into the calculation of slepton pair production to leading order at partonic level and the next-to-leading order result will be stated.

Finally, in chapter 4, the procedure of numerically evaluating the cross sections will be discussed. The different procedures will be explained and showcased such as the Vegas algorithm and the LHAPDF library. This will lead into the results of the thesis and the data will be visualized through different plots.

# Chapter 1

## Basics of Quantum Field Theory

Quantum Field Theory (QFT) is the basis for all current high-energy physics and the development of QFT is what eventually led to the standard model. In this chapter we will look at some basics of QFT, and give an overview of the constructions and the derivation of different Feynman rules. This thesis will not dive too deep into each derivation but will instead sketch an outline in order to provide a basic understanding. For a more detailed and complete introduction to Quantum Field Theory and its consequences, see e.g. [1, 2].

We will begin this chapter with a discussion about group theory where we will introduce the concept of Lie groups and Lie algebras. The different representations one can make from this set of groups will correspond to transformations that we want our physics to be independent under. This will lead us into Yang-Mills theories where we will first briefly discuss the Abelian case, which gives rise to QED, before we finally look at the more generic non-Abelian case. From gauge theory we will find that the gauge bosons that arise from the symmetries will be assumed massless, which has historically caused some criticism and doubts about the formalism. This was rectified later when the concept of particles acquiring mass through spontaneous symmetry breaking was put forward. The chapter will then finish by briefly discussing this mechanism.

### 1.1 Group Theory

This section will give a brief overview of the relevant group theory needed for the discussion in this thesis. We will first give an overview of the most generic definitions of a group before building up Lie groups. We will then later use a specific representation of the group to construct our Yang-Mills theory.

For a group,  $G$ , we define it by the set of group elements  $\{g_i\} \in G$  and a multiplicative rule between the elements  $g_i \circ g_j = g_k$ , which takes two elements in the group and gives a rule as to how they are combined, which gives a third element of the same group. A basic example of this construction is the real numbers  $\mathbb{R}$ , except zero, as elements of the group and regular multiplication as the rule. It is this rule that defines

the group, independent of the concrete representation. This definition also includes a couple of requirements on the multiplication rule of the group. These requirements are associativity of the rule,  $(g_i \circ g_j) \circ g_k = g_i \circ (g_j \circ g_k)$ , that there exists an identity,  $\mathbb{1} \circ g_i = g_i \circ \mathbb{1} = g_i$ , and that the group elements have inverses,  $g_i^{-1} \circ g_i = \mathbb{1}$ , where both the identity and the inverse are members of the group  $\mathbb{1}, g_i^{-1} \in G$ .

So far these group elements are fully abstract objects, but to be able to work with them in a vector space we need a representation that embeds these group elements  $g_i$  into operators that acts on vectors in this space. In our case we will often deal with finite-dimensional representations where these group elements can be embedded into matrices. An example of this kind of representation is the Lorentz group, which is the set of boosts and rotations that keeps the Minkowski metric invariant,  $\Lambda^T g \Lambda = g$ . These  $\Lambda$  matrices are represented in the 4-vector space where they act as transformations on the four vectors as

$$X^\mu \rightarrow \Lambda^\mu_\nu X^\nu. \quad (1.1)$$

An example of a matrix in this representation can be a boost along the  $x$  axis which is represented as

$$\Lambda_x = \begin{pmatrix} \cosh \beta_x & \sinh \beta_x & 0 & 0 \\ \sinh \beta_x & \cosh \beta_x & 0 & 0 \\ 0 & 0 & 1 & 0 \\ 0 & 0 & 0 & 1 \end{pmatrix}. \quad (1.2)$$

This way of writing the Lorentz group into a set of matrices illustrates in particular one representation of this group, and in this case, it is the 4-vector representation. In order to investigate a general representation as desired, we need to first look at the group separate from a specific 4-vector representation. This is made easier by looking at an infinitesimal transformation of the representation. An infinitesimal 4-vector transformation with the infinitesimal rotation angles  $\theta_i$  and boosts  $\beta_i$  can be written as

$$\delta X_0 = \beta_i X_i, \quad (1.3)$$

$$\delta X_i = \beta_i X_0 - \epsilon_{ijk} \theta_j X_k, \quad (1.4)$$

where repeating indices are summed over,  $\beta_i X_i \equiv \sum_i \beta_i X_i$ . Here  $\epsilon_{ijk}$  is the Levi-Civita tensor, defined as  $\epsilon_{123} = 1$  where the interchange of any two indices flips the sign. This can be written in a 4-vector form as

$$\delta X_\mu = i \sum_{i=1}^3 [\theta_i (J_i)_{\mu\nu} + \beta_i (K_i)_{\mu\nu}] X^\nu, \quad (1.5)$$

with  $J_i$  and  $K_i$  being the generators of the group. They can be written as  $4 \times 4$  matrices where

$$J_1 = i \begin{pmatrix} 0 & & & \\ & 0 & & \\ & & 0 & -1 \\ & & 1 & 0 \end{pmatrix}, J_2 = i \begin{pmatrix} 0 & & & \\ & 0 & 1 & \\ & & 0 & \\ -1 & & & 0 \end{pmatrix}, J_3 = i \begin{pmatrix} 0 & & & \\ & 0 & -1 & \\ & 1 & 0 & \\ & & & 0 \end{pmatrix}, \quad (1.6)$$

and

$$K_1 = i \begin{pmatrix} 0 & -1 & & \\ -1 & 0 & & \\ & & 0 & \\ & & & 0 \end{pmatrix}, K_2 = i \begin{pmatrix} 0 & -1 & & \\ & 0 & & \\ -1 & & 0 & \\ & & & 0 \end{pmatrix}, K_3 = i \begin{pmatrix} 0 & & -1 & \\ & 0 & & \\ & & 0 & \\ -1 & & & 0 \end{pmatrix}. \quad (1.7)$$

These matrices are called the generators of the Lorentz group since any element of the group for a specific rotation and boost can be written uniquely as

$$\Lambda = \exp(i\theta_i J_i + i\beta_i K_i). \quad (1.8)$$

An advantage of writing the group elements  $\Lambda$  in this manner is that it is also a completely general way of writing down any group element of any specific representation. As long as the group has a finite dimensional representation, it can always be written as an exponential of the generator matrices. In a more concrete formulation, any members  $g$  in a group  $G$  can be written as  $g = \exp(i\theta^a T^a)$ . Here  $\theta^a$  are real numbers while  $T^a$  are the generic generators of the group. These generators live in what we call an algebra, as we can add or multiply them together, while the group members live in the group, since there is only a multiplication rule. Groups normally also have a name corresponding to the symmetry of the group. For instance, the Lorentz group is sometimes called  $O(1,3)$  because it is an orthogonal group acting on a vector space with a metric,  $g^{\mu\nu}$ , that has a (1,3) signature of  $(+, -, -, -)$ .

### 1.1.1 Lie Groups

We can now turn our attention to a certain class of groups, namely the Lie groups. This a class of groups where every group has an infinite number of elements but only a finite number of generators. This is the class of groups which gives rise to the different forces described in quantum field theory such as QED from the  $U(1)$  group, the weak force from the  $SU(2)$  group and the strong force, QCD, from the  $SU(3)$  group which we will study in more detail in chapter 2. From this description we can note that the Lorentz group will be a Lie group. The generators of the group form the Lie algebra, and these generators can be thought of as the basis of the group. They can also be found for any explicit form of the members  $\Lambda$  by expanding for small changes around the identity  $\mathbb{1}$  like we did to find equation (1.5) and the generators of the Lorentz group.

The Lie algebra, which is formed through the group generators  $T^a$ , is a vector space  $g$  with a multiplication operation known as the Lie bracket. This Lie bracket is a bilinear mapping and can be written formally as

$$[\cdot, \cdot] : g \times g \rightarrow g, \quad (1.9)$$

where  $[\cdot, \cdot]$  is the Lie bracket. For such a vector space to actually be defined as an algebra, then the Jacobi identity has to be fulfilled. This identity is given as

$$[A, [B, C]] + [B, [C, A]] + [C, [A, B]] = 0, \quad (1.10)$$



For all the elements,  $A, B, C$ , of the algebra.

The group generators can be written in terms of the Lie brackets as

$$[T^a, T^b] = if^{abc}T^c, \quad (1.11)$$

where  $f^{abc}$  are known as structure constants of the algebra. We then define a Lie group to be Abelian if the structure constants are all zero, while it is called non-Abelian otherwise. An example of the latter is the Pauli spin group,  $SU(2)$ , which has the algebra  $\mathfrak{su}(2)$  with structure constants  $f^{abc} = \epsilon^{abc}$ , where  $\epsilon^{abc}$  is the totally antisymmetric Levi-Civita tensor with  $\epsilon^{123} = 1$ .

For our purposes, when we embed the group generators in matrices for the physical representation, the Lie bracket can also be referred to as the ordinary commutator. This means we can write the mapping as

$$[A, B] = AB - BA. \quad (1.12)$$

When we can write our mapping in this way it implies that the product of the generators is well defined. This means that the relation  $[A, [B, C]] = ABC - ACB - BCA + CBA$  holds, and from this one can check that the Jacobi identity in (1.10) automatically holds. We can also write the Jacobi identity in terms of structure constants from (1.11) as

$$f^{bcd}f^{ade} + f^{cad}f^{bde} + f^{abd}f^{cde} = 0. \quad (1.13)$$

We will now look at the definitions for the different Lie groups. The first is the unitary group, which is defined as a group that preserves the complex inner product;

$$\langle \vec{\psi}, \vec{\chi} \rangle = \langle \vec{\psi} | U^\dagger U | \vec{\chi} \rangle. \quad (1.14)$$

This means that  $U^\dagger U = \mathbb{1}$ , where  $U$  are elements of the unitary group. The subgroup known as the special unitary group has the additional requirement that  $\det(U) = 1$ . These groups are defined by how they act on a vector space such that  $SU(N)$  is the special unitary group acting on a  $N$ -dimensional vector space. A special unitary group  $SU(N)$  will have in total  $N^2 - 1$  generators, this is then the definition of the dimension of the group, i.e.  $d(G) = N^2 - 1$  for  $G = SU(N)$ .

The special unitary groups will be the groups of interest for us when we will discuss the construction of quantum field theory. In addition to this, we will quickly mention some other Lie groups. Firstly, we have the orthogonal groups that preserves a real inner product defined as

$$\vec{V} \cdot \vec{W} = \vec{V} \cdot O^T O W, \quad (1.15)$$

where  $O^T O = \mathbb{1}$ . These matrices have determinant of  $\pm 1$  while members of  $SO(N)$  have determinant 1. Other Lie groups include the symplectic group, and the five exceptional simple Lie groups,  $G_2, F_4, E_6, E_7$  and  $E_8$ .

### 1.1.2 Representations of $SU(N)$

We will now outline different representations of the  $SU(N)$  groups, which will be important in relating the group to physical complex valued fields that arises in quantum field theory. These  $N$ -dimensional fields will then automatically be invariant under the group transformations. The two most important representations and the two we will cover in this section are the fundamental representation and the adjoint representation.

The fundamental representation of the group is the smallest non-trivial representation and is also often called the defining representation. For the  $SU(N)$  group this representation will be generated by the set of all  $N \times N$  Hermitian matrices that also have a trace of 0. There will then be a set of  $N$  fields,  $\phi_i$ , that transforms in the fundamental representation. An infinitesimal transformation of these fields can be written as

$$\phi_i \rightarrow \phi_i + ib^a (T_{\text{fund}}^a)_{ij} \phi_j, \quad (1.16)$$

for any real numbers  $b^a$ , and  $T_{\text{fund}}^a$  being the generators in the fundamental representation. The complex conjugate fields, however, transform in the anti-fundamental representation but this can be related to the fundamental generators through the infinitesimal transformation

$$\phi_i^* \rightarrow \phi_i^* - ib^a \phi_j^* (T_{\text{fund}}^a)_{ji}, \quad (1.17)$$

so that both the regular and the complex conjugate fields transformations can always be related to the fundamental generators.

Our default and most used representation will be the fundamental one, which leads us to remove the subscript from the generators when we are in this representation,  $T_{\text{fund}}^a = T^a$ . For the adjoint representation (see below) however, we will denote the generators as  $T_{\text{adj}}^a$ .

The algebra of the representation can be determined from an expansion of a basis of group elements around the identity. For  $SU(2)$  you find that the generators in the fundamental representation are the Pauli matrices  $\sigma^a$  normalized by a factor of  $1/2$  so that

$$T^a = \tau^a \equiv \frac{\sigma^a}{2}. \quad (1.18)$$

These Pauli matrices satisfy the definition of a Lie algebra from (1.11) with  $f^{abc} = \epsilon^{abc}$ , which shows that  $SU(2)$  is a non-Abelian group. For  $SU(3)$  it is conventional to write the generators of the fundamental representation in the standard basis  $T^a = \frac{1}{2} \lambda^a$ , where  $\lambda^a$  are the Gell-Mann matrices found by Murray Gell-Mann in 1962 [3], with  $\lambda^3$  and  $\lambda^8$  being diagonal.

For the normalization of these generators, a convention needs to be chosen. A common convention in physics is that the structure constants are normalized by the equation

$$\sum_{c,d} f^{acd} f^{bcd} = N \delta^{ab}. \quad (1.19)$$

This convention leads to a fixed normalization of the generators in any representation since the relation from (1.11) must hold for generators of different representations

with the same structure constants. That relation is also not invariant under rescaling of the generators  $T^a$ . Equation (1.19) implies that the generators of  $SU(N)$  in the fundamental representation is normalized by

$$\text{tr}(T^a T^b) = \frac{1}{2} \delta^{ab}, \quad (1.20)$$

which can be checked explicitly for  $SU(2)$  and  $SU(3)$  from the generators we have already listed.

The next important representation for us is the adjoint representation. This is the representation that acts on the vector space that is spanned by the generators themselves. For  $SU(N)$  there are  $N^2 - 1$  generators, which means that the adjoint representation is an  $N^2 - 1$ -dimensional representation. The definition of the matrices that describes this representation is given by the equation

$$(T_{\text{adj}}^a)^{bc} = -i f^{abc}, \quad (1.21)$$

which for  $SU(2)$  gives the  $3 \times 3$  matrices:

$$T_{\text{adj}}^1 = \begin{pmatrix} 0 & & \\ & 0 & -i \\ & i & 0 \end{pmatrix}, \quad T_{\text{adj}}^2 = \begin{pmatrix} 0 & & i \\ & 0 & 0 \\ -i & & 0 \end{pmatrix}, \quad T_{\text{adj}}^3 = \begin{pmatrix} 0 & -i & \\ i & 0 & \\ & & 0 \end{pmatrix}. \quad (1.22)$$

For  $SU(3)$  we will then have an  $3^2 - 1 = 8$  dimensional representation, so the adjoint representation consists of  $8 \times 8$  matrices. Later we will discuss how the importance of the adjoint representation arises from the gauge fields, and that these fields must transform in the adjoint representation.

Lastly, we will look at the basis independent Casimir invariants which for any representation  $R$  is defined as

$$C_2(R) \equiv \sum_a T_R^a T_R^a, \quad (1.23)$$

and

$$C(R) \delta^{ab} \equiv \text{tr}[T_R^a T_R^b] \quad (1.24)$$

where  $T_R^a$  are the generators of the representation  $R$ . Here  $C_2(R)$  is known as the quadratic Casimir, while  $C(R)$  is the index of the representation. For the fundamental representation we have from (1.20) that

$$C(\text{fund}) = T_F = \frac{1}{2}, \quad (1.25)$$

and for the adjoint representation we will have

$$C(\text{adj}) = C_A = N, \quad (1.26)$$

which comes from  $f^{acd} f^{bcd} = N \delta^{ab}$  with sum over repeating indices being implicit.

To find the quadratic Casimir we can set  $a = b$  in (1.24) and sum over the indices to get

$$d(R)C_2(R) = C(R)d(G), \quad (1.27)$$

with  $d(R)$  being the dimension of the representation and  $d(G)$  the dimension of the group. This implies that the quadratic Casimir in  $SU(N)$  for the fundamental representation is

$$C_2(\text{fund}) = C_F = \frac{T_F d(SU(N))}{d(\text{fund})} = \frac{N^2 - 1}{2N}, \quad (1.28)$$

since  $d(SU(N)) = N^2 - 1$  and  $d(\text{fund}) = N$ . For the adjoint representation we will get

$$C_2(\text{adj}) = C_A = N, \quad (1.29)$$

since the dimension of the representation is the same as the dimension of the group, so the quadratic Casimir is the same as the index in the adjoint representation.

## 1.2 Gauge theory

The most important quantity we have in quantum field theory is the Lagrangian. This is the equation which determines the interactions between the fields in QFT. Gauge theory then tells us that this Lagrangian is invariant under certain local transformations of the Lie groups. This will lead us to be able to uniquely define a Lagrangian that follows from gauge invariance.

In this section we will consider both the Abelian and non-Abelian case of local transformations. For differentiation of the fields, we are moved to introduce a new field that compares different local transformations at two different points. This new field is called a Wilson line and we will show how the introduction of this leads to a covariant derivative and gauge fields.

### 1.2.1 Abelian gauge theory

If we consider as an example a complex scalar field  $\phi(x)$ , then the phase of this field should be just a convention and any phase shift should not affect the theory. Generalizing this to local transformations leads us to the transformation

$$\phi(x) \rightarrow e^{iQ\alpha(x)}\phi(x), \quad (1.30)$$

which the Lagrangian should be invariant under. Here,  $Q$  is an arbitrary charge of the field and  $\alpha(x)$  is the local phase shift. This symmetry is the  $U(1)$  symmetry group of the Lie groups discussed above.

From this we can see that a mass term like  $m^2\phi^*\phi$  automatically is invariant under the transformation. Now let us compare two different points  $x^\mu$  and  $y^\mu$  which are very far away from each other, so any choice for phase transformation at one point will

not have an effect on the field value at the other point. This means that the phase transformation of these two points is dependent on the local phase shifts  $\alpha(x)$  and  $\alpha(y)$ . If we then try to compare these two fields, we get

$$\phi(x) - \phi(y) \rightarrow e^{iQ\alpha(x)}\phi(x) - e^{iQ\alpha(y)}\phi(y). \quad (1.31)$$

In essence, we would get different results for this comparison depending on the convention of phase transformation. Because of this, it would be impossible to define any regular derivative of the field independent from the convention as  $\partial_\mu\phi(x)$ .

If we then want to be able to compare the fields at different points, we need to include a new ingredient. This new component is a new bi-local field  $W(x, y)$  that depends on two points  $x^\mu$  and  $y^\mu$ . This field, referred to as a Wilson line, is what we want to transform as

$$W(x, y) \rightarrow e^{iQ\alpha(x)}W(x, y)e^{-iQ\alpha(y)}. \quad (1.32)$$

From this we result with

$$\begin{aligned} W(x, y)\phi(y) - \phi(x) &\rightarrow e^{iQ\alpha(x)}W(x, y)e^{-iQ\alpha(y)}e^{iQ\alpha(y)}\phi(y) - e^{iQ\alpha(x)}\phi(x) \\ &= e^{iQ\alpha(x)}[W(x, y)\phi(y) - \phi(x)]. \end{aligned} \quad (1.33)$$

From the resulting equation, we notice that  $|W(x, y)\phi(y) - \phi(x)|$  is independent on the choice of phase and this means we can make comparisons between  $\phi(x)$  and  $\phi(y)$  through the Wilson line.

We can now define a new derivative by setting  $y^\mu = x^\mu + \delta x^\mu$ , dividing by  $\delta x^\mu$  and take the limit of  $\delta x^\mu \rightarrow 0$ . Doing this gives the definition of the covariant derivative as

$$D_\mu\phi(x) \equiv \lim_{\delta x^\mu \rightarrow 0} \frac{W(x, x + \delta x)\phi(x + \delta x) - \phi(x)}{\delta x}, \quad (1.34)$$

so that

$$D_\mu\phi(x) \rightarrow e^{iQ\alpha(x)}D_\mu\phi(x), \quad (1.35)$$

which follows from (1.33) for a  $\delta x^\mu$  of any size.

A natural requirement to set now is that  $W(x, x) = 1$ , which means we do not need to do anything to compare fields at the same point. Then, if  $\delta x^\mu$  is small, we should be able to expand  $W(x, x + \delta x)$  around 1 as

$$W(x, x + \delta x) = 1 - ie\delta x^\mu A_\mu(x) + \mathcal{O}(\delta x^2), \quad (1.36)$$

with  $e$  for now being an arbitrary constant, and  $A_\mu(x)$  being the introduction of the gauge field. The transformation of  $A_\mu(x)$  can be determined from the transformation of  $W(x, y)$  in (1.32) as

$$A_\mu(x) \rightarrow A_\mu(x) + \frac{1}{e}\partial_\mu\alpha(x). \quad (1.37)$$

So then the derivative in (1.34) can be written as  $D_\mu\phi = \partial_\mu\phi - ieA_\mu\phi$ . From this we conclude that the gauge field,  $A_\mu$ , is introduced as a connection that compares field values  $\phi$  at different points, independent of their different phases.

Now we can combine what we have noted so far to write down a part of our scalar Lagrangian as

$$\mathcal{L} \supset |D_\mu \phi|^2 + m^2 |\phi|^2. \quad (1.38)$$

This equation is invariant under the transformation in (1.30). What is missing from this Lagrangian now is a kinetic expression for the gauge field  $A_\mu$ . To find this expression we can note that since  $D_\mu \phi$  transforms like the field, then so will also  $D_\mu D_\nu \phi$ . This leads to

$$[D_\mu, D_\nu] \phi(x) \rightarrow e^{iQ\alpha(x)} [D_\mu, D_\nu] \phi(x), \quad (1.39)$$

where  $[D_\mu, D_\nu]$  is the regular commutator bracket. Expanding the commutator, we get

$$[D_\mu, D_\nu] \phi(x) = ([\partial_\mu, \partial_\nu] - ie[\partial_\mu, A_\nu] + ie[\partial_\nu, A_\mu]) \phi(x) = -ieF_{\mu\nu} \phi(x), \quad (1.40)$$

where we have used that  $[A_\mu, A_\nu] = 0$ . Here  $F_{\mu\nu} = \partial_\mu A_\nu - \partial_\nu A_\mu$  is the classical field strength tensor.

From this discussion we now have a new definition of the field strength tensor from the covariant derivatives of the fields as

$$F_{\mu\nu} \equiv \frac{i}{e} [D_\mu, D_\nu]. \quad (1.41)$$

Using this definition, we can find a geometric interpretation of the field strength tensor as the difference of comparing fields as  $D_\mu D_\nu$  compared to the other direction of  $D_\nu D_\mu$ .

With this new term, we can expand our lagrangian to include a kinetic term in the gauge field. The term should then be invariant under the transformation of the gauge field by equation (1.37). We then have our full scalar Abelian Lagrangian as

$$\mathcal{L}_{\text{QED}} = -\frac{1}{4} F_{\mu\nu}^2 + |D_\mu \phi|^2 + m^2 |\phi|^2. \quad (1.42)$$

The QED name comes from the fact that this Lagrangian is the defining Lagrangian for quantum electrodynamics (QED), and as we have seen, it arises from an U(1) symmetry of the fields.

## 1.2.2 Non-Abelian gauge theory

To continue working out the gauge theory we would have to quantize the fields, and from that calculate Feynman rules for interactions and propagators. First we will instead discuss how the same procedure of finding an invariant Lagrangian looks for a non-Abelian gauge theory, where instead of scalar complex fields  $\phi$  we have N-dimensional Dirac fermion field

$$\vec{\psi} = \begin{pmatrix} \psi_1(x) \\ \psi_2(x) \\ \vdots \\ \psi_N(x) \end{pmatrix}. \quad (1.43)$$

where each of the  $\psi_i(x)$  is a Dirac spinor containing a right handed and a left handed Weyl spinor so that

$$\psi_i(x) = \begin{pmatrix} \psi_L(x) \\ \psi_R(x) \end{pmatrix}. \quad (1.44)$$

Here each component of  $\psi$  transforms according to a local  $SU(N)$  symmetry as

$$\psi_i \rightarrow (e^{i\alpha^a(x)T^a})_{ij}\psi_j, \quad (1.45)$$

where the sum over  $j$  is once again implicit, and  $T^a$  are the generators of the symmetry group.

With this construction, the expected invariant contraction of the fields as  $\psi^\dagger\psi$ , turns out to not be invariant. Because of this, we need to introduce another element to the theory, namely the gamma matrices,  $\gamma^\mu$ . If we define  $\bar{\psi} \equiv \psi^\dagger\gamma^0$  with this, we can define an invariant Lorentz scalar as  $\bar{\psi}\psi$ .

This gives us our first invariant term of our non-Abelian Lagrangian as  $\mathcal{L} \supset m\bar{\psi}_j\psi_j$ . For a kinetic term in the fields, we will encounter the same problem as we did for the Abelian case being that we could not compare field values at different points and hence any regular derivatives would not be well defined. We instead want to once again introduce the Wilson line as

$$W(x, y) \rightarrow e^{i\alpha^a(x)T^a}W(x, y)e^{-i\alpha^a(y)T^a}. \quad (1.46)$$

Here we have made use of that  $T^{a\dagger} = T^a$  for generators in  $SU(N)$ .

With this, the expression  $|W(x, y)\bar{\psi}(y) - \bar{\psi}(x)|$  is again invariant under the different local transformation of the fields, and we can use this to define the covariant derivative in the same form as for the Abelian case. We then need to find the infinitesimal expansion of the Wilson line, and using the transformation above we find

$$W(x^\mu, x^\mu + \delta x^\mu) = \mathbb{1} - igA_\mu^a(x)T^a\delta x^\mu. \quad (1.47)$$

If we compare this equation to (1.36), we notice that we pick up the generators of the group. In addition, we need to sum over  $N$  different generators which brings up  $N$  different gauge fields  $A_\mu^a$ . To be able to compare these equations more easily to the case of the Abelian theory and to simplify calculations, we will define  $\mathbf{A}_\mu \equiv A_\mu^a T^a$ . With this notation the covariant derivative becomes

$$D_\mu = \partial_\mu \mathbb{1} - ig\mathbf{A}_\mu, \quad (1.48)$$

which looks exactly like the previous covariant derivative we found after the redefinition of  $\mathbf{A}_\mu$ .

Having this in hand, we get the kinetic term in the Lagrangian to determine all the elements with the Dirac fermion and its interaction with the gauge fields as follows

$$\mathcal{L} = \bar{\psi}_i(\delta_{ij}i\cancel{\partial} + g\mathbf{A}_{ij}^a T_{ij}^a - m\delta_{ij})\psi_j, \quad (1.49)$$

where the terms are written in spinor form, and the slashed notation describes  $\not{\partial} = \gamma^\mu \partial_\mu$ .

The final term we need now is again a kinetic term for the gauge field, which we can find by again considering the definition of the field strength tensor  $F_{\mu\nu}$  from equation (1.41). By inserting the covariant derivative we find ourselves with

$$\mathbf{F}_{\mu\nu} = \frac{i}{g}[D_\mu, D_\nu] = \frac{i}{g}(-ig(\partial_\mu \mathbf{A}_\nu - \partial_\nu \mathbf{A}_\mu) - g^2[\mathbf{A}_\mu, \mathbf{A}_\nu]). \quad (1.50)$$

Now we can use the Lie algebra of the commutators,  $[T^a, T^b] = if^{abc}T^c$ , and then use that  $\mathbf{F}_{\mu\nu} = F_{\mu\nu}^a T^a$  to get that the field strength tensor becomes.

$$F_{\mu\nu}^a = \partial_\mu A_\nu^a - \partial_\nu A_\mu^a + gf^{abc}A_\mu^b A_\nu^c. \quad (1.51)$$

Comparing this to the Abelian case we see that the difference is the structure constants  $f^{abc}$  since in an Abelian group these are defined as  $f^{abc} = 0$ . Inserting this into the field strength tensor we find that  $F_{\mu\nu}^a$  reduces to the classical electromagnetic field strength.

In order to write down an invariant term from the field strength tensor, we need to determine the transformations of the gauge field  $A_\mu^a$ . To derive the transformation we can look at the transformation of the field  $D_\mu \vec{\psi} \rightarrow U \cdot D_\mu \vec{\psi}$  where  $U(x) = \exp(i\alpha^a(x)T^a) \in \text{SU}(N)$  is the group element of a local transformation. Then

$$D'_\mu \vec{\psi}' = (\partial_\mu - ig\mathbf{A}'_\mu) \cdot U \cdot \vec{\psi} = U \cdot (\partial_\mu - ig\mathbf{A}_\mu) \cdot \vec{\psi}, \quad (1.52)$$

with  $\mathbf{A}'_\mu$  being the transformed version of  $\mathbf{A}_\mu$ . Then we get

$$\partial_\mu U - ig\mathbf{A}'_\mu U = -igU\mathbf{A}_\mu. \quad (1.53)$$

Solving this for  $\mathbf{A}'_\mu$  we have

$$\mathbf{A}'_\mu = U\mathbf{A}_\mu U^{-1} - \frac{i}{g}(\partial_\mu U)U^{-1}. \quad (1.54)$$

We can then look at the infinitesimal transformation and view the component form where  $\mathbf{A}_\mu = A_\mu^a T^a$ . This gives the transformation of the gauge field as

$$A_\mu^a(x) \rightarrow A_\mu^a(x) + \frac{1}{g}\partial_\mu \alpha^a(x) - f^{abc}\alpha^b(x)A_\mu^c(x). \quad (1.55)$$

With this we can finally write down the full locally invariant  $\text{SU}(N)$  Lagrangian as

$$\mathcal{L}_{\text{YM}} = -\frac{1}{4}(F_{\mu\nu}^a)^2 + \bar{\psi}_i(\delta_{ij}i\not{\partial} + gA_{ij}^a T_{ij}^a - m\delta_{ij})\psi_j, \quad (1.56)$$

where the subscript YM comes from that this is often referred to as the Yang-Mills Lagrangian. In addition to (1.56) there is another term which is consistent with  $\text{SU}(N)$  invariance that we could add which is

$$\mathcal{L}_\theta = 2\theta\partial_\mu(\epsilon^{\mu\nu\alpha\beta}A_\nu^a F_{\alpha\beta}^a). \quad (1.57)$$



where  $\theta$  is a real number. This term is a total derivative, so it does not contribute to any order in a perturbative theory. Although, thanks to non-perturbative effects, it can contribute in other ways. In quantum chromodynamics for example,  $\theta$  is called the strong  $CP$  phase and would induce an electric dipole moment to the neutron proportional to this phase. The absence of this moment is known as the strong  $CP$  problem. This is beyond the scope of this thesis, but this problem and a proposed solution can be found in, for example [4].

## 1.3 Quantum Yang-Mills theory

To be able to make any predictions in quantum field theory, we need to quantize the fields in question so that they can act on different states in order to create or destroy particles and anti-particles.

In this chapter, the procedure of quantizing the fields and deriving the Feynman rules from them are discussed. This will first be done through a path integral formalism, otherwise known as the Faddeev-Popov procedure. Then the concept of gauge fixing will be reviewed before we end the discussion with presenting the resulting QED rules, and we will generalize to non-Abelian gauge theories.

### 1.3.1 Path integral formulation

In quantum field theory we want to compute interaction matrix elements known as S-matrix elements, and these are time ordered products of fields valued at  $n$  different points as  $\langle \Omega | T \{ \phi(x_1) \phi(x_2) \cdots \phi(x_n) \} | \Omega \rangle$ , with  $|\Omega\rangle$  being the vacuum state of the interaction theory, this is also known as a correlation function. In the path integral formalism, calculating the correlation function is done through the equation

$$\langle \Omega | T \{ \phi(x_1) \cdots \phi(x_n) \} | \Omega \rangle = \frac{\int \mathcal{D}\phi \phi(x_1) \cdots \phi(x_n) e^{iS[\phi]}}{\int \mathcal{D}\phi e^{iS[\phi]}}, \quad (1.58)$$

with  $S[\phi] = \int d^4x \mathcal{L}$  being the classical free action. The  $\mathcal{D}\phi$  means the product of all the fields  $\phi(x)$  with the correct boundary conditions so that

$$\mathcal{D}\phi = d\phi_1(x) \cdots d\phi_n(x). \quad (1.59)$$

In order to compute these correlation functions in quantum field theory, we consider the normal action in the presence of an external classical current  $J(x)$ . This gives rise to a functional called the generating functional which is denoted as

$$Z[J] = \int \mathcal{D}\phi \exp \left\{ iS[\phi] + i \int d^4x J(x) \phi(x) \right\}. \quad (1.60)$$

Then, when  $J = 0$ , this reduces to the vacuum amplitude without any source as

$$Z[0] = \int \mathcal{D}\phi e^{iS[\phi]}. \quad (1.61)$$

From this we can introduce variational partial derivatives and in the end define our correlation function as

$$\langle \Omega | T \{ \phi(x_1) \cdots \phi(x_n) \} | \Omega \rangle = (-i)^n \frac{1}{Z[0]} \left. \frac{\partial^n Z}{\partial J(x_1) \cdots \partial J(x_n)} \right|_{J=0}. \quad (1.62)$$

We now have a systematic way of calculating correlation functions and we can use this to find our Feynman rules by considering different correlation functions. This will be done separately for scalar QED first, then we will outline the main differences for non-Abelian gauge theories, before showing the QCD rules used in chapter 2.

### 1.3.2 Path integrals for scalar Abelian theory

The Lagrangian of interest in scalar quantum electrodynamics was given in equation (1.42) and this consists of kinetic terms of  $\phi$  and  $A_\mu$  in addition to interaction terms. Firstly, to make the fields quantized, we need to make them operator valued by introducing creation and annihilation operators to the fields. Then we can use the above procedure for the correlation function of interest to find the relevant Feynman rules.

Expanding the Lagrangian in (1.42) gives

$$\mathcal{L} = -\frac{1}{4} F_{\mu\nu}^2 - \phi^* (\square + m^2) \phi - ieA^\mu [\phi^* (\partial_\mu \phi) - (\partial_\mu \phi^*) \phi] + e^2 A_\mu^2 |\phi|^2. \quad (1.63)$$

We can then use this on the different correlation functions. For the scalar propagator in the free theory we must calculate

$$\langle 0 | T \{ \phi(x) \phi(y) \} | 0 \rangle = (-1)^2 \frac{1}{Z[0]} \left. \frac{\partial^2 Z[J]}{\partial J(x) \partial J(y)} \right|_{J=0}, \quad (1.64)$$

where the generating functional, omitting terms that will not contribute to the final result, is

$$Z[J] = \int \mathcal{D}\phi \exp \left\{ i \int d^4x \left( -\frac{1}{2} \phi (\square + m^2) \phi + J(x) \phi(x) \right) \right\}. \quad (1.65)$$

This exponential can be turned into a quadratic expression of  $J(x)$  and  $J(y)$  by the use of the relation

$$\int d\vec{p} e^{-\frac{1}{2} \vec{p} A \vec{p} + \vec{J} \vec{p}} = \sqrt{\frac{(2\pi)^n}{\det A}} e^{\frac{1}{2} \vec{J} A^{-1} \vec{J}}, \quad (1.66)$$

with  $A = i(\square + m^2)$ . This gives that the generating functional is

$$Z[J] = N \exp \left\{ -i \int d^4x \int d^4y \frac{1}{2} J(x) \Pi(x-y) J(y) \right\}, \quad (1.67)$$

where  $\Pi(x-y)$  is the solution of  $A^{-1}$  which can be computed through the Green's function as

$$(\square + m^2) \Pi(x-y) = -\delta(x-y), \quad (1.68)$$

which results in

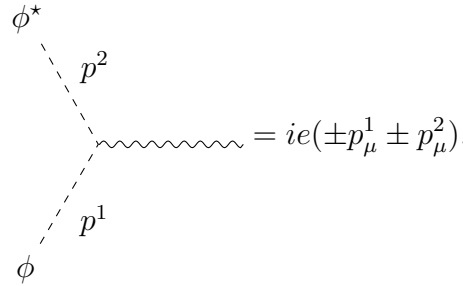
$$\Pi(x-y) = \int \frac{d^4p}{(2\pi)^4} \frac{1}{p^2 - m^2} e^{ip(x-y)}. \quad (1.69)$$

Using all of the above, we can finally compute the correlation function as

$$\begin{aligned} \langle 0|T\{\phi(x)\phi(y)\}|0\rangle &= (-1)^2 \frac{1}{Z[0]} \left. \frac{\partial^2 Z[J]}{\partial J(x)\partial J(y)} \right|_{J=0} \\ &= i\Pi(x-y) \\ &= \int \frac{d^4p}{(2\pi)^4} \frac{i}{p^2 - m^2} e^{ip(x-y)}. \end{aligned}$$

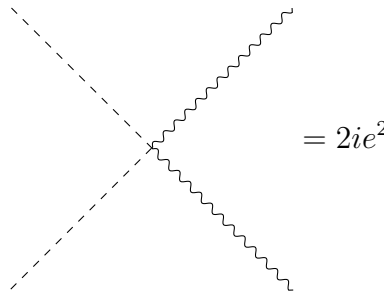
Then in momentum space, this scalar propagator becomes  $\frac{i}{p^2 - m^2}$ .

From the generating functionals, one can see that to find the interacting Feynman rules, one can, in principle, simply read off the terms in front of the chosen interaction vertex, letting derivatives pick up momentum factors. For example, for the three-point vertex of two scalars and the photon field one gets



$$= ie(\pm p_\mu^1 \pm p_\mu^2). \quad (1.70)$$

where the  $\pm$  is dependent on the orientation of the momentum and if the scalar is a real scalar or an anti-scalar. This vertex rule come from the term  $ieA^\mu[\phi^*(\partial_\mu\phi) - (\partial_\mu\phi^*)\phi]$  in the Lagrangian. Then from the term  $e^2A_\mu^2|\phi|^2$ , we get the vertex rule



$$= 2ie^2. \quad (1.71)$$

The final piece of the scalar theory now is the photon propagator. Here we run into a problem where the operator we need to invert has a determinant equal to zero and is thus not invertible. To solve this, the Lagrangian will pick up an extra term called a gauge fixing term of the form  $\frac{1}{2\xi}(\partial_\mu A^\mu)^2$ , where  $\xi$  is a real parameter that any final

physical calculations should be independent of. With this new term the operator will be invertible and the photon propagator becomes

$$\mu \overset{p}{\text{~~~~~}} \nu = -\frac{g_{\mu\nu} - (1 - \xi)\frac{p_\mu p_\nu}{p^2}}{p^2}, \quad (1.72)$$

in which we have used generating functionals. In order to introduce the gauge fixing term in the path integrals, we have divided and multiplied by the function

$$f(\xi) = \int \mathcal{D}\pi e^{-i \int d^4x \frac{1}{2\xi} (\Box\pi)^2} = \int \mathcal{D}\pi e^{-i \int d^4x \frac{1}{2\xi} (\Box\pi - \partial_\mu A^\mu)^2}. \quad (1.73)$$

where the last equation is just a shift in  $\pi$  which leaves the integral unchanged and is therefore independent of  $A^\mu$ . From this, the dependence on the  $\pi$ -field will lead to an overall normalization and drops out of any physical quantities.

### 1.3.3 Quantization of non-Abelian theory

For the non-Abelian theory, the quantization of the particle field propagators and interaction terms follows from the Abelian case in which we can read off the terms of interest from the Lagrangians. There is, however, one big difference in the non-Abelian case for gauge fixing, and it follows from the Faddeev-Popov procedure which is explained in detail in [5].

The consequence of this new method is the introduction of Grassmann valued fields which are known as Faddeev-Popov ghosts. These arise from a constant determinant that cannot be factorized out of the generating functionals. To remedy this, we can use a property of the Grassmann numbers where any determinant can be written as a path integral over Grassmann numbers as

$$\det(\mathcal{O}) = \int \mathcal{D}\bar{\theta}\mathcal{D}\theta \exp\left(-i \int d^4x \bar{\theta}\mathcal{O}\theta\right), \quad (1.74)$$

in which  $\theta$  and  $\bar{\theta}$  are the Grassmann and anti-Grassmann numbers, respectively. The determinant in question here has the form  $\det(\partial^\mu D_\mu)$  so the path integral arising from this is

$$\det(\partial^\mu D_\mu) = \int \mathcal{D}\bar{c}\mathcal{D}c \exp\left(i \int d^4x \bar{c}(-\partial^\mu D_\mu)c\right). \quad (1.75)$$

This then enters into the Lagrangian together with the gauge fixing term to provide the full gauge-fixed path integral for a non-Abelian theory as

$$Z[0] = \text{const.} \times \int \mathcal{D}A\mathcal{D}\psi_i\mathcal{D}\bar{c}\mathcal{D}c \exp\left\{i \int d^4x \left[\mathcal{L}[A, \psi_i] - \frac{1}{2\xi}(\partial_\mu A^{a\mu})^2 - \bar{c}^a \partial^\mu D_\mu c^a\right]\right\}, \quad (1.76)$$

with  $c^a$  and  $\bar{c}^a$  are anticommuting Lorentz scalars, known as the Faddeev-Popov ghosts and anti-ghosts respectively. There is one such pair for each of the gauge fields indexed by  $a$ .

From the exponent of the integral above, we can write the full Faddeev-Popov Lagrangian extending (1.56) as

$$\mathcal{L}_{\text{FP}} = -\frac{1}{4}(F_{\mu\nu}^a)^2 - \frac{1}{2\xi}(\partial^\mu A_\mu^a)^2 + (\partial^\mu \bar{c}^a)(\delta^{ac}\partial_\mu + gf^{abc}A_\mu^b)c^c + \bar{\psi}(i\not{D} - m)\psi. \quad (1.77)$$

The vertex rules that arises from this theory, and specifically from the SU(3) group, are listed in chapter 2.

A final note from this procedure is that the gauge fields in the non-Abelian theory are all assumed massless, but the experimentally discovered gauge bosons  $Z$ ,  $W^+$  and  $W^-$  are all massive. The masses of these bosons have been shown to arise from spontaneous symmetry breaking (SSB) of the vacuum expectation value. This introduces a new boson which was named the Higgs boson. This concept will not be further discussed in this thesis, however a construction of SSB and the Higgs mechanism where these particles pick up masses is given in [6, 7].



# Chapter 2

## From partons to QCD

In this chapter we will discuss the development of the strong interactions of quantum chromodynamics (QCD). This is achieved by starting from the classical Coulomb scattering, then calculate the deep inelastic scattering (DIS) by introducing the parton model before finally deriving the strong interaction from an SU(3) gauge symmetry. This will allow us to derive the Feynman rules of QCD and see how such rules affect the previously calculated scattering result from the parton model at a higher order in perturbation theory

### 2.1 Coulomb scattering

The concept of the existence of small constituents inside the protons originates from Richard Feynman, who stated that there are some objects inside the proton that he called partons and that these are essentially free within the proton [8]. This assertion was used to describe the high energy behavior of electron proton scattering. In this section, we will outline the discussion about electron proton scattering from the low energy limit and then connect this to the theory of quantum chromodynamics and the subsequent discovery of the quarks and gluons.

From the scattering of electrons and protons at lower energy levels one would measure different properties of the proton, and early experiments of electron-proton scattering showed that the proton behaved as a fermion. Given this fermionic behavior we can then use normal Feynman rules for fermionic scattering and find the resulting cross section from these rules. The Feynman diagram corresponding to this interaction is shown in figure 2.1.

This diagram is the leading order diagram for electron proton scattering and in the low energy limit the cross section simplifies to

$$\frac{d\sigma}{d\Omega} = \frac{\alpha^2}{4E^2 \sin^4\left(\frac{\theta}{2}\right)} \frac{E'}{E} \left( \cos^2 \frac{\theta}{2} - \frac{q^2}{2m_p^2} \sin^2 \frac{\theta}{2} \right), \quad (2.1)$$

with  $E$  and  $E'$  being the initial and final energies of the incoming electron,  $q^\mu = k^\mu - k'^\mu$

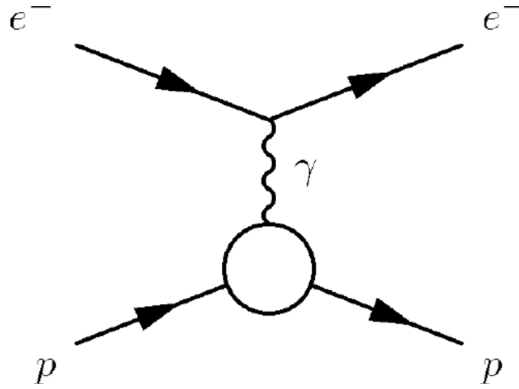


Figure 2.1: Fermionic scattering of electrons and protons mediated by a photon,  $\gamma$ .

being the momentum transfer vector from the electron to the proton,  $\theta$  being the angle between the incoming and outgoing electron, and  $\alpha = e^2/(4\pi)$ . This cross section is the classical Coulomb scattering and has been derived from normal QED rules. By going to higher orders one can find corrections to the Coulomb scattering.

To study more closely the corrections to this scattering, particularly for the proton, we can consider the vertex of an off-shell photon with momenta  $q^\mu$  as being absorbed by the proton with incoming and outgoing momenta  $p^\mu$  and  $p'^\mu$ . Then we can parametrise this vertex to any loop order into form factors  $F_1$  and  $F_2$  because of momentum conservation and the Ward identity [9]. This incoming off-shell photon with momenta will then be absorbed by the proton in a vertex that can be written on the form  $\bar{u}(p')(ie\Gamma^\mu)u(p)$  with  $u(p)$  and  $\bar{u}(p')$  as the incoming and outgoing proton spinors. We can now decompose the  $\Gamma^\mu$  into our form factors as

$$\Gamma^\mu = F_1(q^2)\gamma^\mu + \frac{i\sigma^{\mu\nu}}{2m_p}g_\nu F_2(q^2) \quad (2.2)$$

If we then insert this general vertex as the original vertex in the Feynman rules for computing the matrix element, we will derive the Rosenbluth formula given as

$$\frac{d\sigma}{d\Omega} = \frac{\alpha^2}{4E^2 \sin^4\left(\frac{\theta}{2}\right)} \frac{E'}{E} \left[ \left( F_1^2 - \frac{q^2}{4m_p^2} F_2^2 \right) \cos^2 \frac{\theta}{2} - \frac{q^2}{2m_p^2} (F_1 + F_2)^2 \sin^2 \frac{\theta}{2} \right]. \quad (2.3)$$

In this equation, all the factors can be measured through the cross section's dependence on the energy and angle of the incoming and outgoing electron. We can then use this expression to find the form factors from experimental data. Through this procedure, the first form factor was shown to fit well to data with the expression  $F_1(q^2) \approx 1/(1 - q^2/0.71 \text{ GeV}^2)^2$  [10]. Using the form factor, we find the characteristic size of the proton to be  $r_0 \sim (0.84 \text{ GeV})^{-1} \sim 1 \text{ fm}$ . The experimentally determined form factors and the characteristic size of the proton created the notion that the proton is not actual a point particle but instead is an extended object. This led experimentalists to increase the



energies of the collisions so that they could get more precise measurements and probe deeper into the proton. When energies got higher in the experiments,  $|q^2| > 1 \text{ GeV}^2$ , researchers expected that the scattering would show an even more complicated charge distribution with higher scales. In contrast, the scattering simplified into point like scattering with the increase in energy. So, at high energy levels when the electron probes deep enough into the proton, point like behavior was observed. From this the theory of the parton model was formed by Feynman, which later enabled the discovery of the quarks.

### 2.1.1 Deep inelastic Coulomb scattering

As the energies of the incoming electron increased, the experimental data showed that the scattering was equivalent to that of point like scattering, and at center-of-mass energies above  $m_p$ , the proton would start to break apart in the final state. This led to reactions such as  $e^- p^+ \rightarrow e^- p^+ \pi^0$ . At even higher energies, the proton can break apart completely and reactions such as  $e^- p^+ \rightarrow e^- X$  occur, where  $X$  is any hadron state that the proton can break apart into as long as the baryon number is conserved, was observed.

For the lower energy scattering, we can look at an off-shell photon being absorbed by a proton and then parameterise the cross section using form factors  $F_1(q^2)$  and  $F_2(q^2)$ . However, since the proton now breaks apart at high energies, we can no longer have vertices like  $\bar{u}(p')\gamma^\mu u(p)$  that were necessary for the parametrisation. Instead, we have to look at the process of an off-shell photon being absorbed by the proton and then breaking the proton up into hadronic states.

To parameterise the cross section in these conditions, it is more natural to look at the entire cross section, and not just the photon vertex, in terms of momentum transfer and the proton momenta. Then we can separate the hadronic and the leptonic part of the cross section into two tensors. The kinematics of this calculation are the same for the electron, and we can again define  $E$  and  $E'$  as the incoming and outgoing electron, in addition to  $\theta$  as the scattering angle, and  $k^\mu$  and  $k'^\mu$  as the momenta of the electron. From this we can write the parameterised cross section as

$$\frac{d\sigma^2}{d\Omega dE'} = \frac{\alpha^2}{4\pi m_p q^4} \frac{E}{E'} L^{\mu\nu} W_{\mu\nu}, \quad (2.4)$$

where  $L^{\mu\nu}$  is the leptonic tensor that encodes the  $e^- \rightarrow \gamma^* e^-$  part of the cross section, and  $W_{\mu\nu}$  is the hadronic tensor that encodes the  $\gamma^* p^+ \rightarrow X$  part of the cross section. The leptonic tensor is the unpolarised cross section of electron radiation and therefore is given by the spin-averaged expression of

$$L^{\mu\nu} = \frac{1}{2} \text{Tr}[\not{k}' \gamma^\mu \not{k} \gamma^\nu] = 2(k'^\mu k^\nu + k'^\nu k^\mu - k \cdot k' g^{\mu\nu}). \quad (2.5)$$

This expression is only dependent on the incoming and outgoing momenta of the electron.

The hadronic tensor however is a bit more complicated, as it has to include all the possible states that the proton can disperse into. Once included, the different possible states will then have to be summed over, and the momenta of these hadrons are integrated over. The hadronic tensor can be written as

$$e^2 \epsilon_\mu^* \epsilon_\nu W^{\mu\nu} = \frac{1}{2} \sum_{X, \text{spin}} \int d\Pi_X (2\pi)^4 \delta^4(q + p_p - p_X) \cdot |\mathcal{M}(\gamma^* p^+ \rightarrow X)|. \quad (2.6)$$

Because all the final state hadrons and their momenta are integrated over, the cross section will not depend on any of these.  $W_{\mu\nu}$  will therefore only depend on the momentum of the proton,  $p^\mu$ , and the momentum of the photon,  $q^\mu$ . Since the total cross section is unpolarized, the hadronic tensor has to be symmetric such that  $W^{\mu\nu} = W^{\nu\mu}$ . Additionally, since the final state particles involved are on-shell, the hadronic tensor will also satisfy the Ward identity, which states that  $q_\mu W^{\mu\nu} = 0$ . With these restrictions we can write down the general tensor as

$$W^{\mu\nu} = W_1 \left( -g^{\mu\nu} + \frac{q^\mu q^\nu}{q^2} \right) + W_2 \left( p^\mu - \frac{p \cdot q}{q^2} q^\mu \right) \cdot \left( p^\nu - \frac{p \cdot q}{q^2} q^\nu \right). \quad (2.7)$$

This expression includes the two scalar form functions  $W_1$  and  $W_2$ . These can only depend on the two invariant scalars  $p \cdot q$  and  $q^2$ . The vector  $q$  is spacelike from momentum conservation of the high energy electron, and we therefore have that  $q^2 < 0$ . Because this scalar is negative, it is often a convention to instead write the cross section in terms of  $Q^2 \equiv -q^2$ . Another common variable to use in addition to  $Q^2$  is the dimensionless ratio known as Bjorken  $x$ , which was introduced by James Bjorken in 1969 [11]. This variable is defined as

$$x \equiv \frac{Q^2}{2p \cdot q}. \quad (2.8)$$

We then use these two variables and contract the tensors  $L^{\mu\nu}$  and  $W_{\mu\nu}$  together given in (2.5) and (2.7) before plugging it back in to equation (2.4) to get the cross section in terms of the scattering angle  $\theta$ , which results in

$$\frac{d\sigma^2}{d\Omega dE'} = \frac{\alpha^2}{8\pi E^2 \sin^4 \frac{\theta}{2}} \left[ \frac{m_p}{2} W_2(x, Q) \cos^2 \frac{\theta}{2} + \frac{1}{m_p} W_1(x, Q) \sin^2 \frac{\theta}{2} \right]. \quad (2.9)$$

Again we have defined the expression only in terms of measurable quantities of the incoming and outgoing momenta of the electron, and therefore no information about the final hadronic state  $X$  is needed as it is integrated over in the hadronic tensor. This means that we can measure the structure functions  $W_1$  and  $W_2$  only by experimentally measuring the energies and angles of the scattered electron.

## 2.1.2 Parton Model

Continuing on, we need to deduce what parts of the proton will be interacting with the high energy electron. This is where Feynman introduced what he called the parton model. In this model he suggested that the electron interacts with a single particle for each scattering process, and it is in fact these partons that contributes to the point like scattering. In order to test this model, we need to figure out what the consequences of the parton model are. The elastic scattering between the incoming electron and a single parton inside the proton with mass  $m_q$  then needs to be calculated as well. The parton will also carry some of the momenta of the original proton and at high energies the parton momenta should be almost collinear to the momentum of the proton. Acknowledging this we can write the momentum of these partons as a fraction of the full proton momentum  $\xi p$ , with  $0 \leq \xi \leq 1$ . In addition, the initial momenta of the parton will be called  $p_i^\mu$  and the final momenta is  $p_f^\mu$ . By momentum conservation we can then write, for the parton vertex, that  $p_i^\mu + q^\mu = p_f^\mu$ . If we now square both sides we will get

$$p_i^2 + 2p_i \cdot q + q^2 = p_f^2. \quad (2.10)$$

Now, given that the partons will have almost light like momenta, we can write  $p_i^2 = p_f^2 = m_q^2$ , where  $m_q$  is the mass of the partons. Using this with our previous definition of the fractional momentum and that  $q^2 = -Q^2$  we get

$$\frac{Q^2}{2\xi p \cdot q} = 1 \quad \Rightarrow \quad \frac{x}{\xi} = 1. \quad (2.11)$$

This shows that if we can measure the Bjorken  $x$  of a scattering then we would also automatically have the fraction of the protons momenta that is involved in the scattering with the electron.

Turning our attention now to the partonic cross section, which will be the reaction of  $e^- p_i \rightarrow e^- p_f$  where we assume that the partons are essentially free with the exception of their QED interactions with the photons. The scattering would then be like any other point like scattering and follow the Rosenbluth formula given in Eq. 2.3 with the form factors  $F_1 = 1$  and  $F_2 = 0$ . If we do not integrate over the energy of the final state electron, this cross section will then take the form

$$\left( \frac{d\sigma(e^- q \rightarrow e^- q)}{d\Omega dE'} \right)_{lab} = \frac{\alpha_e^2 Q_i^2}{4E^2 \sin^4 \frac{\theta}{2}} \left[ \cos^2 \frac{\theta}{2} + \frac{Q^2}{2m_q^2} \sin^2 \frac{\theta}{2} \right] \delta \left( E - E' - \frac{Q^2}{2m_q} \right), \quad (2.12)$$

where  $Q_i$  is the QED charge of the interacting parton. The assumption of free point like partons is why there are no extra generic form factors  $F_{1,2}(Q)$  in front of the sine and cosine terms, as it was for the low energy limit of the electron proton scattering. This is because the elastic scattering of the electron and parton, given the weakly interacting state of these partons with photons, is expected to have a small logarithmic dependence on  $Q^2$  when the initial partonic momentum  $p_i$  is fixed. This scale dependence comes from the fact that the partons are point like objects, unlike the proton that has a size,

and therefore we result with the structure functions. When we have a fixed  $p_i$ , then we would also have a fixed  $x$ , according to equation 2.11. This experimentally observed relative independence of  $Q^2$  at a fixed value for  $x$  is known as Bjorken scaling [11], and it is one of the essential results from the parton model.

The last thing we now need to get a precise prediction for the Bjorken scaling in the parton model, is a procedure on how to deal with the question of which parton the virtual photon will exchange with. For this we must consider the wavefunctions of the partons inside the proton and the timescale that the photon is probing. Since the momenta of the proton sloshes around its constituents at a timescale roughly equal to the inverse of its mass,  $\sim \Lambda_{QCD}^{-1} \sim m_p^{-1}$ , and the timescale the photon probes is around the inverse of the exchange energy  $\sim Q^{-1}$ , we can notice that this time scale is significantly smaller than the sloshing of momenta in the proton. Because the scales are several orders of magnitude apart,  $Q \gg \Lambda_{QCD}$ , this allows us to treat the parton wavefunctions as decoherent, i.e. independent. This means that we can adopt a probabilistic interpretation and then introduce the classic probability  $f_i(\xi)d\xi$  that the photon hits parton  $i$ , which carries a fraction  $\xi$  of the proton momentum.

### 2.1.3 Parton distribution functions

The functions  $f_i(\xi)$  (mentioned above) are called parton distribution functions (PDFs). With these functions we can make more precise statements as to the calculations of the interacting partons. We do also have some constraints on these functions given that they should be probabilities of some kind. For example if the proton had one down quark,  $d$ , then this quark needs to carry some momentum and  $\int d\xi f_d(\xi) = 1$ . However, inside the proton we can have several virtual quark anti-quark pairs and gluons. But we can use the fact that quark numbers are conserved in both QED and QCD interactions, so the proton will have a total down-quark number of 1, up-quark number of 2 and any other quark number as 0, and this gives the relations

$$\begin{aligned} \int d\xi [f_d(\xi) - f_{\bar{d}}(\xi)] &= 1, \\ \int d\xi [f_u(\xi) - f_{\bar{u}}(\xi)] &= 2, \\ \int d\xi [f_i(\xi) - f_{\bar{i}}(\xi)] &= 0. \end{aligned} \tag{2.13}$$

Here  $\bar{d}$  is the down anti-quark,  $u$  and  $\bar{u}$  are the up quark and anti-quark, and  $i$  and  $\bar{i}$  are the rest of the so-called sea quarks, which are the strange, charm and bottom quarks. However, for the gluon, there is no conserved number, so there is no further sum rules corresponding to  $f_g$ . Lastly, we have momentum conservation which gives the final rule as

$$\sum_j \int d\xi [\xi f_j(\xi)] = 1, \tag{2.14}$$

where the sum here is over all partons.

In order to determine the PDFs, it is required to do a global fit to not only data from DIS experiments, but also many other high energy processes such as  $p\bar{p}$  and  $pp$  collisions, the latter of which we will focus on later in this thesis.

Now we shall take a step back and look at the original assumption of the parton model. This assumption is that a cross section of the form  $e^-p^+ \rightarrow e^-X$ , with  $X$  being any final hadronic state, is given by the partonic scattering of  $e^-p_i \rightarrow e^-X$ , where the parton  $p_i$  carries the momentum  $p_i^\mu = \xi p^\mu$ , and we integrate over the momentum fraction  $\xi$ . This gives

$$\sigma(e^-p^+ \rightarrow e^-X) = \sum_i \int_0^1 d\xi f_i(\xi) \hat{\sigma}(e^-p_i \rightarrow e^-X). \quad (2.15)$$

Here we introduce the convention of adding circumflexes to the partonic level cross section.

Now we can compare this equation to the DIS equation given in equation (2.9) by inserting in to the partonic level cross section we found in (2.12). Since we are integrating over the incoming quark momenta, we can also use that in the lab frame, the proton is at rest and the relation  $p_i^\mu = \xi p^\mu$  to infer that the effective mass of the parton must be also given by  $m_q = \xi m_p$ . This results in

$$\begin{aligned} \left( \frac{d\sigma(e^-P^+ \rightarrow e^-X)}{d\Omega dE'} \right)_{lab} &= \sum_i \int_0^1 d\xi f_i(\xi) \frac{\alpha^2 Q_i^2}{4E^2 \sin^4 \frac{\theta}{2}} \left[ \cos^2 \frac{\theta}{2} + \frac{Q^2}{2(\xi m_p)^2} \sin^2 \frac{\theta}{2} \right] \\ &\times \delta \left( E - E' - \frac{Q^2}{2\xi m_p} \right). \end{aligned} \quad (2.16)$$

To compute this integral we can note that since  $q^\mu = (E - E', \vec{k} - \vec{k}')$ . Then the Lorentz invariant quantity of

$$\nu \equiv \frac{p \cdot q}{m_p}, \quad (2.17)$$

would be reduced to the energy lost by the electron in the rest frame of the proton, which is also the same frame as lab frame. So that

$$\frac{p \cdot q}{m_p} = (E - E')_{lab}, \quad (2.18)$$

since in the proton rest frame we have that  $p^\mu = (m_p, \vec{0})$ . We can then insert the definition of Bjorken  $x$  from equation (2.8) to get that

$$E - E' = \frac{Q^2}{2m_p x}. \quad (2.19)$$

Using this relation, the delta function becomes

$$\delta \left( E - E' - \frac{Q^2}{2\xi m_p} \right) = \delta \left( \frac{Q^2}{2xm_p} - \frac{Q^2}{2\xi m_p} \right) = \frac{2m_p}{Q^2} x^2 \delta(\xi - x). \quad (2.20)$$

Now we can insert the expression for the delta function back into (2.16) and perform the integral, which, because of the delta function, boils down to the replacement  $\xi \rightarrow x$ , and we get

$$\left( \frac{d\sigma(e^-P^+ \rightarrow e^-X)}{d\Omega dE'} \right)_{lab} = \sum_i f_i(\xi) \frac{\alpha^2 Q_i^2}{4E^2 \sin^4 \frac{\theta}{2}} \left[ \frac{2m_p}{Q^2} x^2 \cos^2 \frac{\theta}{2} + \frac{1}{m_p} \sin^2 \frac{\theta}{2} \right]. \quad (2.21)$$

We can now compare this result to the form factors we introduced in (2.9), and we see that

$$\begin{aligned} W_1(x, Q) &= 2\pi \sum_i Q_i^2 f_i(x), \\ W_2(x, Q) &= 8\pi \frac{x^2}{Q^2} \sum_i Q_i f_i(x). \end{aligned} \quad (2.22)$$

This gives us the final prediction for Bjorken scaling, and it shows that the quantities  $W_1(x, Q)$  and  $Q^2 W_2(x, Q)$  are indeed independent of  $Q$  at a fixed  $x$ . We can also notice that there exists a ratio between  $W_1$  and  $W_2$  given by  $W_1(x, Q) = \frac{Q^2}{4x^2} W_2(x, Q)$ . This relation is known as the Callan-Gross relation [12]. A demonstration of the predicted Bjorken scaling was shown by the Particle Data Group [13] and is visualized here in figure (2.2)

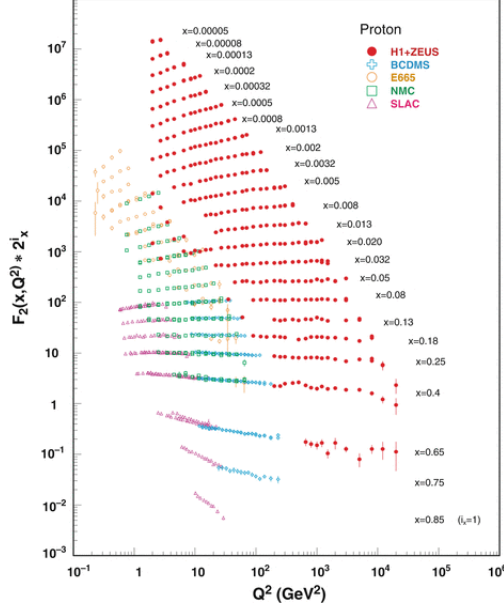


Figure 2.2: Demonstration of Bjorken scaling by the Particle Data Group from 2012. Here the structure function  $F_2(x, Q^2)$  is related to our  $W_2(x, Q)$  through the relation  $F_2(x, Q^2) = \frac{Q^2}{2x} W_2(x, Q)$ . In addition, it is multiplied by  $2^{i_x}$ , where  $i_x$  is the number of the  $x$  bin. From the function we see that  $x = 0.85$  corresponds to  $i_x = 1$ , while  $x = 0.00005$  would correspond to  $i_x = 24$ .

## 2.2 Quantum chromodynamics and DIS

In this section we will look at quantum chromodynamics (QCD) from a group theory perspective and utilize what we have learned from chapter 1. This will lead us to derive the Feynman rules of the QCD theory, and finally we can calculate the deep inelastic scattering result from a perturbative quantum chromodynamics perspective to next-to-leading order. This will then allow us to make a prediction about Bjorken scaling at higher orders in perturbative QCD where it is in fact not fully independent of the energy scale  $Q^2$ , but instead contain a weak logarithmic dependence on  $Q^2$ .

### 2.2.1 QCD from gauge theories

Quantum chromodynamics is a gauge theory formed from the local transformations of the  $SU(3)$  group. Here the fermionic fields with spin 1/2 are called quarks, and the gauge fields are called gluons with spin 1. The quarks carry an extra quantum number in the form of colour that corresponds to the charge of the group.

The quark fields live in the fundamental representation of the group, this vector space is called colour space, and is written as a triplet

$$\vec{\psi}(x) = \begin{pmatrix} \psi_1(x) \\ \psi_2(x) \\ \psi_3(x) \end{pmatrix}. \quad (2.23)$$

We have already seen that the triplet will transform under local gauge transformations as

$$\vec{\psi}(x) = U(x)\vec{\psi}(x), \quad (2.24)$$

with

$$U(x) = e^{i\alpha^a(x)T^a}. \quad (2.25)$$

$T^a$  are, in the  $SU(3)$  case,  $3 \times 3$  hermitian matrices, while  $\alpha^a(x)$  are real numbers.

The generators are traceless and form a basis for  $SU(3)$ , so we know that the index  $a$  will sum over eight values  $a = 1, \dots, 3^2 - 1 = 8$ . This implies that there exists three different coloured quarks and eight gluons. However, it has been discovered experimentally that there are three different families of quarks represented as  $SU(2)$  quark doublets

$$\begin{pmatrix} u \\ d \end{pmatrix}, \quad \begin{pmatrix} c \\ s \end{pmatrix}, \quad \begin{pmatrix} t \\ b \end{pmatrix}. \quad (2.26)$$

So in total we have 18 different coloured quark states. Though for scattering processes we will sum over the contributions of the quarks, so we will not need to explicitly state which specific quark is in the interaction.

The generators of the  $SU(3)$  Lie group will satisfy the Lie algebra defined in (1.11) as a commutation relation  $[T^a, T^b] = if^{abc}T^c$ . In section 1.1 we also defined Casimir

invariants such as the quadratic Casimir  $C_2(R)$  and the index of the representation  $C(R)$ . The definition of these were given in (1.23) and (1.24) respectively.

In the fundamental representation for the quarks we get

$$\begin{aligned} C(\text{fund}) &= T_F = \frac{1}{2}, \\ C_2(\text{fund}) &= C_F = \frac{4}{3}, \end{aligned} \quad (2.27)$$

and in the adjoint representation for the gluons we get

$$C(\text{adj}) = C_2(\text{adj}) = C_A = 3. \quad (2.28)$$

The full locally SU(3)-invariant Lagrangian of QCD containing the interactions and the kinematics of the quarks and gluons is

$$\mathcal{L} = -\frac{1}{4}(F_{\mu\nu}^a)^2 - \frac{1}{2\xi}(\partial^\mu A_\mu^a)^2 + (\partial^\mu \bar{c}^a)(\delta^{ac}\partial_\mu + gf^{abc}A_\mu^b)c^c + \bar{\psi}(i\not{D} - m)\psi, \quad (2.29)$$

where  $c^a$  and  $\bar{c}^a$  are the so-called ghost and anti-ghost fields respectively that appear from the Faddeev-Popov procedure. Additionally, a summation over the quark flavors  $\alpha = u, d, s, c, t, b$  and the color  $i = 1, 2, 3$  is understood, so that  $\psi = (\psi_{\alpha i})$ . The term  $\frac{1}{2\xi}(\partial^\mu A_\mu)^2$  comes from the gauge fixing term discussed in section 1.3.

In order to derive the Feynman rule from this Lagrangian, we need to expand the field strength tensor by using equation (1.51). This is a tedious process but in the end, the kinetic terms of the QCD Lagrangian are shown to be

$$\mathcal{L}_{\text{kin}} = -\frac{1}{4}(\partial_\mu A_\nu^a - \partial_\nu A_\mu^a)^2 - \frac{1}{2\xi}(\partial^\mu A_\mu^a)^2 + \bar{\psi}(i\not{D} - m)\psi - \bar{c}^a \square c^a \quad (2.30)$$

The corresponding propagators of these terms can be read off the Lagrangian through the procedure of finding the equations of motions for the given particle and then finding the Greens function of the operator we end up with. This gives

$$\nu; b \text{ } \underbrace{\hspace{2cm}} \text{ } \mu; a = i \frac{-g^{\mu\nu} + (1 - \xi) \frac{p^\mu p^\nu}{p^2}}{p^2 + i\varepsilon} \delta^{ab}, \quad (2.31)$$

$$j \longrightarrow i = \frac{i\delta^{ij}}{\not{p} - m + i\varepsilon}, \quad (2.32)$$

$$b \text{ } \dots \text{ } a = \frac{i\delta^{ab}}{p^2 + i\varepsilon}, \quad (2.33)$$

for the gluon, quark, and ghosts respectively.

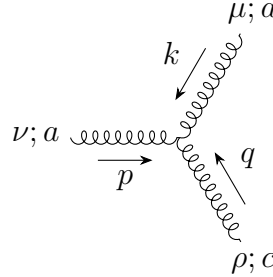
The vertex rules can be found by reading off the interaction Lagrangian, which we noticed in the previous chapter when discussing the path integral formalism in section 1.3. The interaction Lagrangian we get from equation (2.30) is

$$\begin{aligned} \mathcal{L}_{\text{int}} &= -gf^{abc}(\partial_\mu A_\nu^a)A^{\mu,b}A^{\nu,c} - \frac{1}{4}g^2(f^{abe}A_\mu^a A_\nu^b)(f^{cde}A^{\mu,c}A^{\nu,d}) \\ &\quad + gf^{abc}(\partial_\mu \bar{c}^a)A^{\mu,b}c^c + gA_\mu^a \bar{\psi} \gamma^\mu T^a \psi. \end{aligned} \quad (2.34)$$



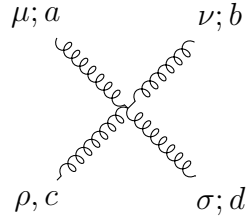
From this expression we can see that there will be a triple- and a four-gluon vertex in addition to the quark-quark-gluon and the ghost-ghost-gluon vertex.

For the triple-gluon vertex, the derivative can act on any of the gluons giving the Feynman rule as



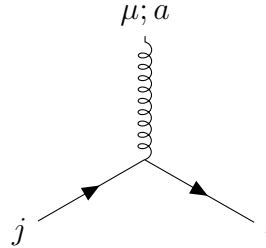
$$= g f^{abc} [g^{\mu\nu}(k-p)^\rho + g^{\nu\rho}(p-q)^\mu + g^{\rho\mu}(q-k)^\nu], \quad (2.35)$$

where all the momenta is taken as incoming,  $p + k + q = 0$ . Then for the four-gluon vertex we have



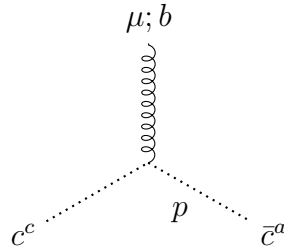
$$= -ig^2 \times [f^{abc} f^{cde} (g^{\mu\rho} g^{\nu\sigma} - g^{\mu\sigma} g^{\nu\rho}) + f^{abc} f^{cde} (g^{\mu\rho} g^{\nu\sigma} - g^{\mu\sigma} g^{\nu\rho}) + f^{abc} f^{cde} (g^{\mu\rho} g^{\nu\sigma} - g^{\mu\sigma} g^{\nu\rho})], \quad (2.36)$$

and the quark-gluon vertex becomes



$$= ig\gamma^\mu T_{ij}^a, \quad (2.37)$$

and finally



$$= -gf^{abc} p^\mu, \quad (2.38)$$

as the ghost-gluon vertex of QCD. In this thesis we will not go to a high enough order in perturbation theory to have a need for ghosts, but we have included them here for completeness sake. We can also notice that from the quark-gluon vertex, where the color of the incoming quark is  $i$  and color of the outgoing quark is  $j$ , can change the color of the quark through the interaction with a gluon as it depends on if the generator  $T_{ij}^a$  is diagonal or not.

## 2.2.2 Deep inelastic scattering from QCD

As we now have the needed Feynman rules from QCD, we can again turn our attention back to the electron-proton scattering. This was previously calculated from the parton model, which assumes free particles inside the proton and that only one of these interact with the electron in the scattering process. We can then parametrize the cross section in a leptonic and a hadronic tensor. It was this hadronic tensor that contained the quantities  $W_1$  and  $W_2$ , which we found to be roughly independent of  $Q^2$  for a fixed value of the Bjorken  $x$ . This came from the property known as Bjorken scaling. However, from figure (2.2), we can notice that there is still some weak dependence on  $Q^2$ , which would imply that there is more to the theory than just the parton model.

Due to these observations, we will combine the parton model with a perturbative calculation in QCD in order to show this dependence of  $Q^2$ . This means we will assume that the parton model still holds, but will then identify these partons with the quarks from QCD. Recalling then, from the previous section, that the hadronic tensor,  $W^{\mu\nu}$ , was given by the vertex  $\gamma^* p^+ \rightarrow X$  where we summed over the final states,  $X$ . We will now instead write  $\hat{W}^{\mu\nu}(z, Q)$  as the partonic version of the hadronic tensor which encodes the vertex  $\gamma^* q \rightarrow X$  integrated over the final states.  $z$  is here the partonic version of  $x$  from (2.8) and is defined by

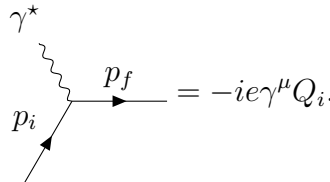
$$z \equiv \frac{Q^2}{2p_i \cdot q}. \quad (2.39)$$

Here  $p_i$  is still the momenta of the parton, or rather the quark, that interacts with the incoming photon.

We can now use the assumption from the parton model that the probability of parton  $i$  having a given fractional momenta  $p_i^\mu = \xi p^\mu$  for some fraction  $0 \leq \xi \leq 1$ , is given by a PDF  $f_i(\xi)$ . We then have that  $x = z\xi$  and we must integrate over  $\xi$  to get the hadronic tensor

$$\begin{aligned} W^{\mu\nu}(x, Q) &= \sum_i \int_0^1 dz \int_0^1 d\xi f_i(\xi) \hat{W}^{\mu\nu}(z, Q) \delta(x - z\xi) \\ &= \sum_i \int_x^1 \frac{d\xi}{\xi} f_i(\xi) \hat{W}^{\mu\nu}\left(\frac{x}{\xi}, Q\right). \end{aligned} \quad (2.40)$$

We can calculate this to leading order in QCD. Here, the only partonic process contributing to  $\hat{W}$  is the process  $\gamma^* q \rightarrow q$ , which becomes



$$= -ie\gamma^\mu Q_i. \quad (2.41)$$

Using the definition of the hadronic tensor given above, the tensor then becomes

$$\begin{aligned}\hat{W}^{\mu\nu}(z, Q) &= \frac{Q_i^2}{2} \int \frac{d^3\vec{p}_f}{(2\pi)^3} \frac{1}{2E_f} \text{Tr} \left[ \gamma^\mu \not{p}_i \gamma^\nu \not{p}_f \right] (2\pi)^4 \delta^4(p_i + q - p_f) \\ &= 2\pi Q_i^2 \left[ \left( -g^{\mu\nu} + \frac{q^\mu q^\nu}{q^2} \right) + \frac{4z}{Q^2} \left( p_i^\mu - \frac{p_i \cdot q}{q^2} q^\mu \right) \cdot \left( p_i^\nu - \frac{p_i \cdot q}{q^2} q^\nu \right) \right] \delta(1-z).\end{aligned}\quad (2.42)$$

We can now read out the quantities  $\hat{W}_1$  and  $\hat{W}_2$  by comparing to the definition of the hadronic tensor in (2.7). This gives

$$\hat{W}_1 = 2\pi Q_i^2 \delta(1-z), \quad (2.43)$$

$$\hat{W}_2 = 8\pi \frac{z}{Q^2} Q_i^2 \delta(1-z). \quad (2.44)$$

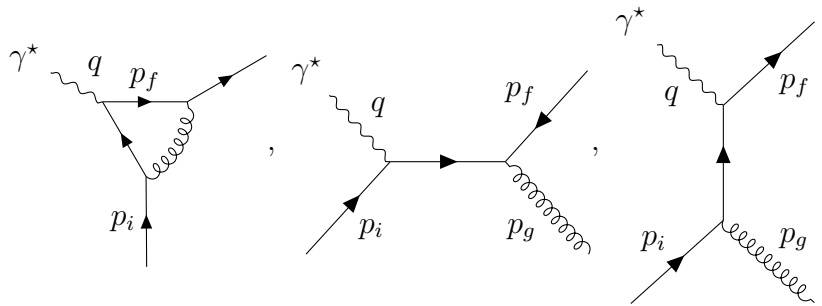
Comparing these quantities to each other confirms the Callan-Gross relation [12]. By plugging each of the structure functions into (2.40) they will separately reproduce (2.22). This shows that the definition of the partonic hadronic tensor is valid from the parton model up to leading order in QCD.

Going forward now to find corrections to Bjorken scaling, we will consider the contracted structure function  $W_0 \equiv -g^{\mu\nu} W_{\mu\nu}$  which presents as

$$W_0(x, Q) = 3W_1(x, Q) - W_2(x, Q) \left( m_p^2 + \frac{Q^2}{4x^2} \right). \quad (2.45)$$

In the high energy limit,  $Q \gg m_p$ , this simplifies to  $W_0(x, Q) = 3W_1 - \frac{Q^2}{4x^2} W_2$ . To leading order at parton level this is  $\hat{W}_0^{\text{LO}} = 4\pi Q_i^2 \delta(1-z)$ .

Going to next-to-leading order in QCD we will pick up one virtual contribution to  $\gamma^* q \rightarrow q$ , in addition to  $s$ - and  $t$ -channel graphs of  $\gamma^* q \rightarrow qg$  as:



$$(2.46)$$

The virtual graph can be calculated through dimensional regularization by going to  $d = 4 - \varepsilon$  dimension. This will, however, lead to UV divergences. These can be removed through renormalization of the free parameters of the theory such as the fields,  $\psi$  and  $A_\mu$ , the different masses, and the charges  $e$  and  $g$ . The interference between the leading order graph and the virtual loop with the counter term diagram is

$$\hat{W}_0^V = 4\pi Q_i^2 \frac{\alpha_s}{2\pi} C_F \left( \frac{4\pi\mu^2}{Q^2} \right)^{\frac{\varepsilon}{2}} \frac{\Gamma(1-\frac{\varepsilon}{2})}{\Gamma(1-\varepsilon)} \left( -\frac{8}{\varepsilon^2} - \frac{6}{\varepsilon} - 8 - \frac{\pi^2}{3} \right) \delta(1-z), \quad (2.47)$$

where terms that will not contribute when  $\varepsilon \rightarrow 0$  have been omitted and  $\alpha_s = g^2/(4\pi)$  is called the strong coupling constant. Since we have included the counter term results, any  $\varepsilon$  poles will be IR divergences.

The calculations of the two real emission graphs are a bit more challenging, as we would have to integrate over the phase space of both the quarks and the gluon and the result is found in [14]. Here we will simply give the result from the above reference as

$$\begin{aligned} \hat{W}_0^R = & 4\pi Q_i^2 \frac{\alpha_s}{2\pi} C_F \left( \frac{4\pi\mu^2}{Q^2} \right)^{\frac{\varepsilon}{2}} \frac{\Gamma(1 - \frac{\varepsilon}{2})}{\Gamma(1 - \varepsilon)} \\ & \times \left[ 3z + z^{\frac{\varepsilon}{2}}(1-z)^{-\frac{\varepsilon}{2}} \cdot \left( -\frac{2}{\varepsilon} \frac{1+z^2}{1-z} + 3 - z - \frac{3}{2} \frac{1}{1-z} - \frac{7}{4} \frac{\varepsilon}{1-z} \right) \right]. \end{aligned} \quad (2.48)$$

Looking at the expressions for the virtual and real emission graphs, it would appear that the virtual graph has a  $\frac{1}{\varepsilon^2}$  double pole while the real emission graphs only have a single pole. However, the real emission result indeed has a double pole. This appears in the terms that include  $\frac{1}{1-z}(1-z)^{-\frac{\varepsilon}{2}}$ . To see this we will consider the identity

$$\frac{1}{(1-z)^{1+\varepsilon}} = -\frac{1}{\varepsilon} \delta(1-z) + \frac{1}{[1-z]_+} - \varepsilon \left[ \frac{\ln(1-z)}{1-z} \right]_+ + \sum_{n=2}^{\infty} \frac{(-\varepsilon)^n}{n!} \left[ \frac{\ln^n(1-z)}{1-z} \right]_+. \quad (2.49)$$

Here we have introduced two plus functions which are defined as

$$\int_0^1 dz \frac{f(z)}{[1-z]_+} \equiv \int_0^1 dz \frac{f(z) - f(1)}{1-z}, \quad (2.50)$$

$$\int_0^1 dz f(z) \left[ \frac{\ln^n(1-z)}{1-z} \right]_+ \equiv \int_0^1 dz (f(z) - f(1)) \frac{\ln^n(1-z)}{1-z}. \quad (2.51)$$

so that in general for our two functions  $[g(z)]_+ = g(z)$  for  $z \neq 1$ .

We can now insert this identity into the real emission result to get

$$\begin{aligned} \hat{W}_0^R = & 4\pi Q_i^2 \frac{\alpha_s}{2\pi} C_F \left( \frac{4\pi\mu^2}{Q^2} \right)^{\frac{\varepsilon}{2}} \frac{\Gamma(1 - \frac{\varepsilon}{2})}{\Gamma(1 - \varepsilon)} \times \left\{ 3 + 2z - \frac{1+z^2}{1-z} \ln(z) + \left( \frac{8}{\varepsilon^2} + \frac{3}{\varepsilon} + \frac{7}{2} \right) \delta(1-z) \right. \\ & \left. - \left( 2 \frac{1+z^2}{\varepsilon} + \frac{3}{2} \right) \left[ \frac{1}{1-z} \right]_+ + (1+z^2) \left[ \frac{\ln(1-z)}{1-z} \right]_+ \right\}. \end{aligned} \quad (2.52)$$

where we observe the double pole of the real emission result, and that it will perfectly cancel with the double pole from the virtual graph.

We can now plug these together with the leading order result to find the form factor

$\hat{W}_0$  up to next-to-leading order as

$$\begin{aligned} \hat{W}_0 = \hat{W}_0^{\text{LO}} + \hat{W}_0^{\text{V}} + \hat{W}_0^{\text{R}} = 4\pi Q_i^2 \left\{ \delta(1-z) - \frac{1}{\varepsilon} \frac{\alpha_s}{\pi} P_{qq}(z) \left( \frac{4\pi\mu^2}{Q^2} \right)^{\frac{\varepsilon}{2}} \frac{\Gamma(1-\frac{\varepsilon}{2})}{\Gamma(1-\varepsilon)} \right. \\ \left. + \frac{\alpha_s}{2\pi} C_F \left[ (1+z^2) \left[ \frac{\ln(1-z)}{1-z} \right]_+ - \frac{3}{2} \frac{1}{[1-z]_+} \right. \right. \\ \left. \left. - \frac{1+z^2}{1-z} \ln z + 3 + 2z - \left( \frac{9}{2} + \frac{1}{3}\pi^2 \right) \delta(1-z) \right] \right\}, \quad (2.53) \end{aligned}$$

with

$$P_{qq}(z) = C_F \left[ (1+z^2) \frac{1}{[1-z]_+} + \frac{3}{2} \delta(1-z) \right]. \quad (2.54)$$

This distribution,  $P_{qq}(z)$ , is known as a DGLAP splitting function after Dokshitzer, Gribov, Lipatov, Altarelli and Parisi [15, 16, 17].

Now we have cancelled the double pole, but we are still left with a single pole in the partonic cross section. This itself is inconsequential as long as the pole drops out of physical predictions. To see how the pole vanishes, we will be considering the infinite part of  $\hat{W}_0$  separately and inserting this into the expression for the total  $W_0$  from equation (2.40). Doing so, we result with

$$W_0(x, Q) = 4\pi \sum_i Q_i^2 \int_x^1 \frac{d\xi}{\xi} f_i(\xi) \left[ -\frac{\alpha_s}{2\pi} P_{qq} \left( \frac{x}{\xi} \right) \left( \frac{2}{\varepsilon} + \ln \frac{\tilde{\mu}^2}{Q^2} \right) + \text{finite} \right], \quad (2.55)$$

where  $\tilde{\mu}^2 \equiv 4\pi e^{-\gamma_E} \mu^2$ . Now, from the definition of plus functions, the DGLAP splitting function satisfies

$$\int_0^1 P_{qq}(z) dz = 0, \quad (2.56)$$

and then by integrating  $W_0$  over  $x$ , the single pole will exactly cancel for a total cross section at a given  $Q$ .

For a fixed  $x$  however, the single pole does not vanish, and  $W_0$  is divergent. We will instead consider differences to get finite answers and the difference in  $W_0(x, Q)$  at a fixed  $x$ , but different energy scales  $Q$  and  $Q_0$  is written as

$$W_0(x, Q) - W_0(x, Q_0) = 4\pi \sum_i Q_i^2 \int_x^1 \frac{d\xi}{\xi} f_i(\xi) \left[ \frac{\alpha_s}{2\pi} P_{qq} \left( \frac{x}{\xi} \right) \ln \frac{Q^2}{Q_0^2} \right]. \quad (2.57)$$

This integral is finite and hence the difference between  $W_0(x, Q)$  at different energy scales are also finite. We then see that as the finite part of equation (2.53) drops out of such differences, it is instead the single pole at parton level that contributes to predictions of logarithmic  $Q$  dependence in the hadronic tensor.

The reason we must consider differences here, even though QCD is a renormalizable theory, is firstly because we have not introduced any cut offs at some physical scale in

order to remove the IR divergences. This is reasonable due to the notion that for low energy scattering, these partons are bound in the proton and does not interact with the incoming electron. The IR divergences can also be absorbed into the definitions of the PDFs and will be handled separately from the partonic cross section. In addition, the difference of  $W_0$  gives a more practical calculation, and we get an answer that we can test. From the result we can see that Bjorken scaling does in fact no longer hold to higher order in perturbative QCD theory as seen in figure 2.2.

## 2.3 Factorization of the PDFs

In our calculation of the deep inelastic scattering cross section, we have already used factorization so that we can write the cross section as a convolution between a perturbative hard calculation,  $H$ , and the parton distribution functions,  $f$ , as

$$\sigma = f \otimes H. \quad (2.58)$$

This way of writing the cross section assumes that factorization is allowed, so that we can treat the PDFs and the perturbative cross section independent of each other. Hence for any scattering process, we can use the same PDFs for different perturbative calculations. This factorization has only been proven to work in a few cases, including the deep inelastic scattering that we have previously considered, and the Drell-Yan process in which a lepton pair is produced from  $pp$  or  $p\bar{p}$  collisions via a gauge boson.

For a full discussion about the proof of factorization, one can read the article by John Collins [18]. In this section, however, we will only briefly outline the process of proving factorization before showing the consequence of factorization in the Drell-Yan case.

### 2.3.1 Outline of factorization proof

In the approach to show factorization in the DIS case, we can relate the cross section to a product of currents  $J^\mu(x)J^\nu(y)$ . We can then rewrite this in terms of local operators before expanding around  $x^\mu = y^\mu$  since in the DIS limit where  $Q^2 \rightarrow \infty$  then  $x^\mu - y^\mu \rightarrow 0$ . Finally, we can define the PDFs as a matrix element of these local operators with proton states as  $f \sim \langle P | \mathcal{O} | P \rangle$ , where  $|P\rangle$  is the proton state.

We want to use the electromagnetic current defined as  $J^\mu(x) = \bar{\psi}(x)\gamma^\mu\psi(x)$  to write the hadronic tensor in terms of a product of this current. For DIS, this means that we write the matrix element as the current at  $x = 0$ , as it couples to an initial proton state  $|P\rangle$  and an arbitrary final hadronic state  $\langle X|$  as

$$\mathcal{M}(\gamma^* p^+ \rightarrow X) = e e^\mu \langle X | J_\mu(0) | P \rangle. \quad (2.59)$$

Then we can compare this to (2.6), and after integrating over the phase space of the final hadronic state using

$$\langle P | J_\mu(0) | X \rangle = e^{-i(p_p - p_X)x} \langle P | J_\mu(x) | X \rangle, \quad (2.60)$$

we get that

$$W_{\mu\nu}(\omega, Q) = \int d^4x e^{iq \cdot x} \langle P | J_\mu(x) J_\nu(0) | P \rangle, \quad (2.61)$$

where  $\omega = 1/x > 1$ .

We now want to write this by using operator product expansion to expand in the  $Q \rightarrow \infty$  limit around  $x^\mu = 0$ . However, in order to complete this, we first need to turn our product of operators into a time-ordered product by using the optical theorem [19]. This theorem states that the total rate for  $\gamma^* p^+ \rightarrow X$  is given as the imaginary part of the forward scattering rate  $\gamma^* p^+ \rightarrow \gamma^* p^+$  so we can write

$$W_{\mu\nu} = 2\text{Im}T_{\mu\nu}, \quad (2.62)$$

with

$$T_{\mu\nu}(\omega, Q) = i \int d^4x e^{iq \cdot x} \langle P | T \{ J_\mu(x) J_\nu(0) \} | P \rangle. \quad (2.63)$$

We can now use operator product expansion (OPE) on this new time ordered product. For our case we use the definition of OPE given as

$$\int d^4x e^{iqx} \mathcal{O}(x) \mathcal{O}(0) = \sum_n C_n(q) \mathcal{O}_n(0). \quad (2.64)$$

We can then write the product of the  $J_\mu(x)$  in the high energy limit as

$$T \{ J^\mu(x) J^\nu(y) \} = \sum_n C_n(x-y) \mathcal{O}_n^{\mu\nu}(x). \quad (2.65)$$

From this there are a bit of tedious calculations that are also outlined in section 32.4 in Schwartz [2]. These calculations eventually lead to an expression for  $T^{\mu\nu}$  as

$$T^{\mu\nu} = \sum_q Q_q^2 \left\{ \left( -g^{\mu\nu} + \frac{q^\mu q^\nu}{q^2} \right) \sum_{n=2,4,\dots}^{\infty} \omega^n \mathcal{A}_q^n + \frac{4}{Q^2 \omega^2} \left( p^\mu - \frac{p \cdot q}{q^2} q^\mu \right) \cdot \left( p^\nu - \frac{p \cdot q}{q^2} q^\nu \right) \sum_{n=2,4,\dots}^{\infty} \omega^n \mathcal{A}_q^n \right\}, \quad (2.66)$$

where  $\mathcal{A}_q^n$  are complex functions of  $Q$ . From this we can again recognize structure functions that we now call  $T_1$  and  $T_2$  as

$$T_1 = \frac{\omega}{2} T_2 = \sum_q Q_q^2 \left( \sum_{n=2,4,\dots}^{\infty} \omega^n \mathcal{A}_q^n \right). \quad (2.67)$$

These structure functions are often related to the dimensionless form factors of the partonic cross section through  $W_1 = 2\text{Im}T_1$  and  $W_2 = \frac{4x}{Q^2} \text{Im}T_2$ . From this we can finally

find an operator definition of the PDFs through the relation  $W_1 = 2\pi \sum_q Q_q^2 f_q(x)$ . This gives

$$f_q(x) = \frac{1}{\pi} \sum_{n=2,4,\dots} x^{-n} \text{Im} \mathcal{A}_q^n. \quad (2.68)$$

This relation gives us an operator definition of the PDFs in the DIS scheme, and can therefore use factorization and write the PDFs separately from the partonic cross section. For the Drell-Yan case, factorization will lead to us being able to write a cross section of the form  $pp \rightarrow l\bar{l}$  as

$$\sigma = \sum_{ab} \int dx_a \int dx_b f_a(x_a) f_b(x_b) \sigma_{ab}, \quad (2.69)$$

where we sum over the partons  $a$  and  $b$ . This will be discussed more in the next chapter.





# Chapter 3

## Beyond the standard model

Although the standard model has been extremely successful in describing the high energy interactions between the fundamental particles, there are still problems that the model cannot explain, such as how to include gravity and the concepts of dark matter and dark energy. Physicists often attempt to solve these problems by adding new theories on top of the existing model. In this chapter, we will consider one of these expansions, namely supersymmetry.

We will begin with a brief overview of this new extension to the standard model, listing the new particles included in this theory and providing the vertex rules for some of these. Then, when we have the necessary Feynman rules, we will consider a Drell-Yan cross section for proton-proton collision that produces a slepton pair, which are the supersymmetric partners of the leptons. We will discuss the kinematics of such a collision before deriving the leading order contribution to the cross section. Finally, we will note how to expand this to higher order in perturbation theory and then recite the next-to-leading order result for the cross section given in the article by Bozzi, Giuseppe and Fuks [20].

### 3.1 Supersymmetry

The model of supersymmetry arises from a symmetry that turns fermions into bosons and bosons into fermions. This model was developed from trying to combine the Poincaré symmetry of special relativity with the local gauge symmetry of QFT into one big symmetry. This extension to include fermion-boson symmetry was named the super-Poincaré algebra [21].

The consequence of fermions now being able to be turned into bosons and vice versa gave rise to a plethora of new particles. In this thesis we will consider the minimal supersymmetric standard model (MSSM) [22] that connects each of the particles of the standard model with its own supersymmetric partner. The complete set of particles in the theory are listed in table 3.1. This table shows how the spin- $\frac{1}{2}$  fermions are mapped to scalar superpartners while the spin-1 bosons and scalar Higgs boson are mapped to

spin- $\frac{1}{2}$  superpartners.

Particle	Symbol	Spin	Superpartner	Symbol	Spin
Quarks	$q$	$\frac{1}{2}$	Squarks	$\tilde{q}$	0
Leptons	$l$	$\frac{1}{2}$	Sleptons	$\tilde{l}$	0
$W_{\text{SU}(2)}$	$W^\pm$	1	Wino	$\tilde{W}^\pm$	$\frac{1}{2}$
$B_{\text{U}(1)}$	$B$	1	Bino	$\tilde{B}$	$\frac{1}{2}$
Gluon	$g$	1	Gluino	$\tilde{g}$	$\frac{1}{2}$
Higgs	$h_u, h_d$	0	Higgsinos	$\tilde{h}_u, \tilde{h}_d$	$\frac{1}{2}$

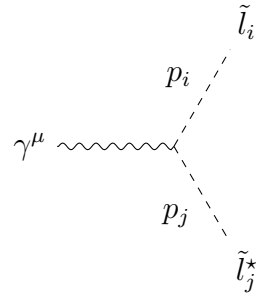
Table 3.1: List of the original particles of the standard model together with their superpartner from the MSSM.

In the table above, the W bosons are the gauge fields of SU(2) and the B boson is the gauge field of U(1). The physical gauge bosons,  $W^\pm, Z$  and the photon,  $\gamma$ , are linear combinations of these. This mixing of bosons is a fundamental part of the electroweak theory and is treated in detail by Weinberg's work in [23]. An additional thing to note from this is the existence of two Higgs boson SU(2) doublets and two Higgsino doublets. This is caused by a gauge anomaly arising with only one Higgsino doublet. Additionally, in the MSSM theory the up type quark and the down type quark no longer coupled to the same Higgs field. So, to make both the up and the down type quark massive, two Higgs fields needs to be introduced in the theory. In the standard model, the bino and wino bosons mix, but now the two Higgsino fields will also mix.

This new MSSM theory adds many new parameters to the standard model and in the unconstrained version of MSSM, there are over 100 new parameters. With all of these parameters, any complete phenomenological analysis of the parameter space is next to impossible. Instead, considering the three assumptions of no new source of CP-violation, no flavour changing neutral currents and first- and second-generation universality, the amount of new parameters compared to the standard model can be reduced to 19. This model is called the phenomenological MSSM [24], and it includes all the new particle masses, the ratio of the vacuum expectation value of the two higgs doublets, and three third generation trilinear couplings.

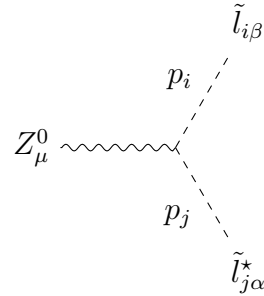
In this thesis we will focus on the sleptons, and how they couple to the particles from the standard model. Specifically we will consider the couplings of these sleptons to the  $Z^0$  boson and the photon, which are what we need later when we are going to calculate the leading order contribution to slepton pair production. A discussion on the Lagrangian of the MSSM and an overview the Feynman rules of the model can be

found in [25]. The vertices of note for us are



$$= ie\delta^{ij}(p_i + p_j)^\mu, \quad (3.1)$$

and



$$= \frac{ig}{\cos(\theta_W)} Z_{l_i}^{\alpha\beta} (p_i + p_j)^\mu, \quad (3.2)$$

where  $\theta_W$  is the Weinberg angle which is the mixing angle between the photon and the  $Z^0$  boson,  $g = \frac{e}{2\sin(\theta_W)}$  is the weak charge and

$$Z_{l_i}^{\alpha\beta} = \frac{1}{2}(L_{1\alpha}^i L_{1\beta}^i - 2\sin^2\theta_W \delta^{\alpha\beta}). \quad (3.3)$$

Here  $\alpha$  and  $\beta$  are the mass states while

$$L^i = \begin{pmatrix} \cos\theta^i & \sin\theta^i \\ -\sin\theta^i & \cos\theta^i \end{pmatrix}, \quad (3.4)$$

is the lepton mixing matrix giving the mixing between the slepton gauge interaction states and their mass eigenstates. Here  $i = \tilde{e}, \tilde{\mu}, \tilde{\tau}$ , where for the selectron and smuon, the mass states and the interaction states are the same so there is no mixing, and therefore  $\theta^{\tilde{e},\tilde{\mu}} = 0$ . These Feynman rules with slepton mixing conventions can be found in [26].

The slepton-photon and the slepton- $Z^0$  vertices are the two vertices needed to calculate the matrix element to leading order later in this chapter. From this calculation we will see that the cross section will depend on the masses of the sleptons and for the stau case, the cross section will also depend on the mixing angle that mixes the interaction states with the physical mass states of the stau particle. From this discussion we have all the pieces necessary for calculating the Drell-Yan process of  $pp \rightarrow \tilde{l}_i \tilde{l}_i$ , which we will do in the next section.

## 3.2 Slepton pair production at LHC

In this section we will discuss the calculation of slepton pair production using the Feynman rules from the previous section. We can then use the factorization theorem in QCD to write our unpolarized cross section as

$$\sigma = \sum_{a,b} \int dM^2 \int_0^1 dx_a \int_0^1 dx_b f_a(x_a, \mu_F^2) f_b(x_b, \mu_F^2) \frac{d\hat{\sigma}_{ab}(z, M^2, \alpha_s(\mu_R))}{dM^2}. \quad (3.5)$$

Here,  $\mu_F$  is introduced as a factorization scale,  $\mu_R$  is a renormalization scale that determines the value of  $\alpha_s$ , and the sum runs over the partons in the proton. The invariant mass of the slepton pair is defined as  $M^2 = z x_a x_b S = z s$  with  $s$  being the partonic center-of-mass energy; this definition can then be used to define the differential cross section in terms of  $z$  as

$$\frac{d\hat{\sigma}}{dM^2} = \frac{d\hat{\sigma}}{dz} \frac{dz}{dM^2} = \frac{d\hat{\sigma}}{dz} \frac{1}{s}. \quad (3.6)$$

The partonic hard scattering cross section can then be calculated in perturbative QCD theory as

$$\frac{d\hat{\sigma}_{ab}}{dz} = \sum_{n=0}^{\infty} \left( \frac{\alpha_s(\mu_R)}{\pi} \right)^n \frac{d\sigma_{ab}^{(n)}}{dz}, \quad (3.7)$$

where  $\sigma^{(n)}$  is the  $n$ -th order coefficient. In this thesis we will focus on the LO ( $n = 0$ ) coefficient, and the results of the NLO ( $n = 1$ ) coefficient will also be stated.

### 3.2.1 Kinematics of the cross section

Here we will consider the kinematics of our process, and to leading order, this simplifies to a  $2 \rightarrow 2$  scattering. With this we can do several simplifications to the kinematics side of the equation by the use of momentum conservation and explicitly performing the phase space integral.

In general, a scattering process can be written as

$$d\sigma = \frac{1}{(2E_1)(2E_2)|\vec{v}_1 - \vec{v}_2|} |\mathcal{M}|^2 (2\pi)^4 \delta^4(\Sigma p_i^\mu - \Sigma p_f^\mu) \times \prod_{\text{final states } j} \frac{d^3 p_j}{(2\pi)^3} \frac{1}{2E_{p_j}}, \quad (3.8)$$

with

$$d\Pi_{\text{LIPS}} = (2\pi)^4 \delta^4(\Sigma p_i^\mu - \Sigma p_f^\mu) \times \prod_{\text{final states } j} \frac{d^3 p_j}{(2\pi)^3} \frac{1}{2E_{p_j}}, \quad (3.9)$$

being referred to the Lorentz-invariant phase space. In this equation,  $|\mathcal{M}|^2$  encodes all the interactions between the particles, and everything else deals with the kinematics of the scattering. Additionally, anything with a subscript 1 or 2 indicates the two incoming particles.

For our specific  $2 \rightarrow 2$  process of  $q\bar{q} \rightarrow \tilde{l}_i \tilde{l}_j^*$ , it is beneficial to consider the center-of-mass (CM) frame where we have that  $\vec{p}_1 = -\vec{p}_2$  and  $\vec{p}_3 = -\vec{p}_4$ . We can also relate the energies as  $E_1 + E_2 = E_3 + E_4 = E_{\text{CM}}$ , with  $E_{\text{CM}}$  being the total energy of the collision in the CM frame. This center-of-mass energy is often written as  $E_{\text{CM}} = \sqrt{S}$ , and we will use this convention from here. Then the phase space becomes

$$d\Pi_{\text{LIPS}} = (2\pi)^4 \delta^4(\Sigma p) \frac{d^3 p_3}{(2\pi)^3} \frac{1}{2E_3} \frac{d^3 p_4}{(2\pi)^3} \frac{1}{2E_4}, \quad (3.10)$$

where  $\Sigma p = \Sigma p_i - \Sigma p_f$ . We can then integrate over  $\vec{p}_4$  by the use of the delta function to get

$$d\Pi_{\text{LIPS}} = \frac{1}{16\pi^2} d\Omega \int dp_f \frac{p_f^2}{E_3 E_4} \frac{1}{E_4} \delta(E_3 + E_4 - \sqrt{S}), \quad (3.11)$$

with  $p_f = |\vec{p}_3| = |\vec{p}_4|$ ,  $E_3 = \sqrt{m_3^2 + p_f^2}$  and  $E_4 = \sqrt{m_4^2 + p_f^2}$ . To continue on from here, one can do a change of variables in the remaining delta function from  $p_f$  to  $x(p_f) = E_3(p_f) + E_4(p_f) - \sqrt{S}$ . By doing this calculation after inserting the Jacobi determinant, one finds that the phase space becomes

$$d\Pi_{\text{LIPS}} = \frac{1}{16\pi^2} d\Omega \frac{p_f}{\sqrt{S}} \theta(\sqrt{S} - m_3 - m_4), \quad (3.12)$$

where  $\theta(\dots)$  is the Heaviside function which is defined as  $\theta(x) = 1$  if  $x > 0$  and 0 otherwise. We can also use that

$$|\vec{v}_1 - \vec{v}_2| = \left| \frac{|\vec{p}_1|}{E_1} + \frac{|\vec{p}_2|}{E_2} \right| = p_i \frac{\sqrt{S}}{E_1 E_2}, \quad (3.13)$$

with  $p_i = |\vec{p}_1| = |\vec{p}_2|$ .

If we then insert both (3.12) and (3.13) into the general equation for the scattering process given in (3.8), we get a relation for the differential scattering in the center-of-mass frame as

$$\left( \frac{d\sigma}{d\Omega} \right)_{\text{CM}} = \frac{1}{64\pi^2 S} \frac{p_f}{p_i} |\mathcal{M}|^2 \theta(\sqrt{S} - m_3 - m_4), \quad (3.14)$$

where the CM subscript reminds us that this is only valid if we work in the center-of-mass frame.

In this equation, the Heaviside function acts as a cutoff so that any processes where the incoming particles do not have enough energy to create the two outgoing particles are cancelled out. We are going to include this as a limit on the invariant mass where this invariant mass is defined in the CM frame as

$$M^2 = (p_3 + p_4)^2 = m_3^2 + m_4^2 + 2E_3 E_4 + 2|\vec{p}_3||\vec{p}_4|. \quad (3.15)$$

Therefore  $M^2 > (m_3 + m_4)^2$ , and if not then we set  $\sigma = 0$ .

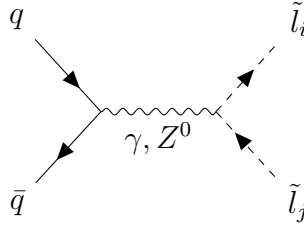
In the next part we will focus on the interaction matrix  $\mathcal{M}$  to find the full cross section. In addition, in the high energy limit of our calculation, we can consider the

incoming quarks as massless so that  $m_1 = m_2 = 0$ . This then gives  $p_i = E_1 = E_2 = \sqrt{S}/4$ . With this, the cross section simplifies to

$$\left(\frac{d\sigma}{d\Omega}\right)_{\text{CM}} = \frac{p_f}{16\pi^2 S^{\frac{3}{2}}} |\mathcal{M}|^2. \quad (3.16)$$

### 3.2.2 Calculation of the LO Drell-Yan cross section

The partonic Feynman diagram of interest when computing the matrix element of our collision is given as the reaction  $q\bar{q} \rightarrow \tilde{l}_i\tilde{l}_j$  at leading order. The diagram can be represented as



with either a photon or a  $Z^0$  boson as the virtual particle.

From this we can see that the matrix element will be a sum of the two contributions as

$$i\mathcal{M} = i\mathcal{M}_\gamma + i\mathcal{M}_{Z^0}, \quad (3.17)$$

and the squared matrix element will consist of three terms as

$$|\mathcal{M}|^2 = |\mathcal{M}_\gamma|^2 + 2\mathcal{M}_\gamma\mathcal{M}_{Z^0}^* + |\mathcal{M}_{Z^0}|^2. \quad (3.18)$$

Here, the first term is the squared photon contribution, the second is the photon- $Z^0$  interference, while the last is the squared  $Z^0$  contribution.

Then by looking at each graph separately, we get for the photon contribution that

$$i\mathcal{M}_\gamma = \bar{v}(p_2)(-iQ_q\gamma^\mu)u(p_1) \frac{-i \left[ g_{\mu\nu} - (1 - \xi) \frac{k_\mu k_\nu}{k^2} \right]}{k^2} (-iQ_l\delta^{ij}(p_i + p_j)^\nu), \quad (3.19)$$

where  $k^\mu = p_1^\mu + p_2^\mu$  and  $k^2 = Q^2 = s$  as the partonic center-of-mass energy, and  $Q_q$  and  $Q_l$  being the charge of the quark and sleptons. According to gauge invariance, the  $\frac{k_\mu k_\nu}{k^2}$  term should not contribute. If we use the equations of motions  $\not{p}_1 u(p_1) = m u(p_1)$  and  $\bar{v}(p_2)\not{p}_2 = -m\bar{v}(p_2)$  and then compute the expression  $\bar{v}(p_2)\gamma^\mu u(p_1)k_\mu$ , this will indeed cancel out and not contribute. Then we get

$$\mathcal{M}_\gamma = \frac{e^2}{s} \delta^{ij} e_q e_l \bar{v}(p_2) \gamma^\mu u(p_1) (p_i + p_j)_\mu, \quad (3.20)$$

and the conjugate amplitude as

$$\mathcal{M}_\gamma^\dagger = \frac{e^2}{s} \delta^{ij} e_q e_l (p_i + p_j)_\mu \bar{u}(p_1) \gamma^\mu v(p_2). \quad (3.21)$$

These spinors,  $u$  and  $v$  have a spin dependence which we need to average over, using the spin sum rule of

$$\sum_s u(p_1)\bar{u}(p_1) = (\not{p}_1 + m_q\mathbb{1}), \quad (3.22)$$

and

$$\sum_s v(p_2)\bar{v}(p_2) = (\not{p}_2 + m_q\mathbb{1}). \quad (3.23)$$

We will also be working in the high energy limit where we can treat the incoming quarks as massless, so  $m_q = 0$ .

With all of this, when calculating the squared matrix element, we will end up with a trace over gamma matrices. We will therefore need to make use the trace identities of

$$\text{Tr}(\gamma^\alpha\gamma^\beta\gamma^\rho\gamma^\sigma) = 4(g^{\alpha\beta}g^{\rho\sigma} - g^{\alpha\rho}g^{\beta\sigma} + g^{\alpha\sigma}g^{\beta\rho}), \quad (3.24)$$

and

$$\text{Tr}(\gamma^\alpha\gamma^\beta) = 4g^{\alpha\beta}, \quad (3.25)$$

together with the fact that the trace of any odd number of these gamma matrices is zero. In addition, we need to average over each of the polarizations of the incoming quark and anti-quark pair. Thus we have to add a factor of  $\frac{1}{4}$  to the squared matrix element which becomes

$$\frac{1}{4} \sum_{\text{spins}} |\mathcal{M}_\gamma|^2 = \frac{e^4}{4s^2} \delta^{ij} e_q^2 e_l^2 \text{Tr}(\not{p}_1 \gamma^\mu \not{p}_2 \gamma^\nu) (p_i + p_j)_\mu (p_i + p_j)_\nu. \quad (3.26)$$

This gives

$$\frac{1}{4} \sum_{\text{spins}} |\mathcal{M}_\gamma|^2 = \frac{e^4}{s^2} \delta^{ij} e_q^2 e_l^2 (p_1^\mu p_2^\nu + p_1^\nu p_2^\mu - p_{12} g^{\mu\nu}) (p_i + p_j)_\mu (p_i + p_j)_\nu, \quad (3.27)$$

where  $p_{12} \equiv p_1 \cdot p_2 = p_1^\mu p_{2\mu}$

The next steps in the calculations are to contract the momenta with each other. This can be simplified further by introducing the Mandelstam variables [27]. These variables can be related to the energies and momenta in the center-of-mass frame. With this, one can insert the matrix element into our expression for the differential cross section to integrate over the solid angles  $\Omega$ . Finally, the cross section can be made differential in the partonic Bjorken  $z$  by adding it as a delta function. However, as we will see later, for the leading order contribution this will just be equivalent of setting  $z = 1$ . These calculations are a bit extensive, but lead to

$$\left( \frac{d\sigma_{qq}^0}{dz} \right)_{\gamma, \text{CM}} = \frac{\alpha^2 \pi \beta^3}{9M^2} e_q^2 e_l^2 \delta^{ij} \delta(1-z), \quad (3.28)$$



as the partonic center-of-mass result, which agrees with the squared photon contribution from [20]. Here we have factorized the slepton mass terms in

$$\beta = \sqrt{1 + \frac{m_i^4}{M^4} + \frac{m_j^4}{M^4} - 2 \left( \frac{m_i^2}{M^2} + \frac{m_j^2}{M^2} + \frac{m_i^2 m_j^2}{M^4} \right)}, \quad (3.29)$$

and  $M^2 = s$  as the partonic center-of-mass energy. From here we will only consider the center-of-mass frame, so the subscript CM will now be implicit.

For both the photon- $Z^0$  interference and the squared  $Z^0$  contribution, one has to go through similar calculations. In the end, the leading order partonic coefficient can be found as

$$\begin{aligned} \frac{d\sigma_{q\bar{q}}^0}{dz} = \frac{\alpha^2 \pi \beta^3}{9M^2} & \left( e_q^2 e_l^2 \delta^{ij} + \frac{e_q e_l \delta^{ij} (L_{Zqq} + R_{Zqq}) \text{Re}[L_{Z\tilde{l}_i \tilde{l}_j} + R_{Z\tilde{l}_i \tilde{l}_j}]}{4 \sin^2 \theta_W (1 - \sin^2 \theta_W) (1 - m_Z^2/M^2)} \right. \\ & \left. + \frac{(L_{Zqq}^2 + R_{Zqq}^2) |L_{Z\tilde{l}_i \tilde{l}_j} + R_{Z\tilde{l}_i \tilde{l}_j}|^2}{32 \sin^4 \theta_W (1 - \sin^2 \theta_W)^2 (1 - m_Z^2/M^2)^2} \right) \delta(1 - z). \end{aligned} \quad (3.30)$$

Here the  $Z^0$  couplings are given as

$$L_{Zqq} = 2T_q^3 - 2e_q \sin^2 \theta_W, \quad R_{Zqq} = -2e_q \sin^2 \theta_W, \quad (3.31)$$

and

$$L_{Z\tilde{l}_i \tilde{l}_j} = (2T_l^3 - 2e_l \sin^2 \theta_W) L_{i1}^{\tilde{l}} L_{j1}^{\tilde{l}}, \quad R_{Z\tilde{l}_i \tilde{l}_j} = -2e_l \sin^2 \theta_W L_{i2}^{\tilde{l}} L_{j2}^{\tilde{l}}, \quad (3.32)$$

where

$$L^{\tilde{l}} = \begin{pmatrix} \cos \theta_{\tilde{l}} & \sin \theta_{\tilde{l}} \\ -\sin \theta_{\tilde{l}} & \cos \theta_{\tilde{l}} \end{pmatrix}, \quad (3.33)$$

is the slepton diagonal mass matrix with  $\theta_{\tilde{l}} = 0$  for both the selectron and the smuon as in equation (3.4), and  $T_f^3$  is the weak isospin charge of the quarks and sleptons.

### 3.2.3 NLO results for slepton pair production

Going to next-to-leading order will generate in total ten new graphs that contribute at this order. These are three QCD loop corrections, three SUSY-QCD loop corrections, two real gluon emission graphs, and two graphs that have one incoming quark and one incoming gluon. In this thesis, these graphs will not be computed analytically but we will numerically evaluate them, so the resulting cross sections will be stated here. The QCD quark-antiquark corrections are [20]

$$\begin{aligned} \frac{d\sigma_{q\bar{q}}^{(1;\text{QCD})}}{dz} = \sigma_0(M^2) C_F & \left[ \left( \frac{\pi^2}{3} - 4 \right) \delta(1 - z) + 4 \left( \frac{\ln(1 - z)}{1 - z} \right)_+ - \frac{1 + z^2}{1 - z} \ln z \right. \\ & \left. - 2(1 + z) \ln(1 - z) + \frac{2P_{qq}^{(0)}(z)}{C_F} \ln \frac{M^2}{\mu_F^2} \right], \end{aligned} \quad (3.34)$$

and the quark-gluon corrections

$$\frac{d\sigma_{qg}^{(1;\text{QCD})}}{dz} = \sigma_0(M^2)T_F \left[ \left( \frac{1}{2} - z + z^2 \right) \ln \frac{(1-z)^2}{z} + \frac{1}{4} + \frac{3z}{2} - \frac{7z^2}{4} + \frac{P_{qg}^{(0)}(z)}{T_F} \ln \frac{M^2}{\mu_F} \right]. \quad (3.35)$$

Here the  $\sigma_0(M^2)$  is the Born cross section given in (3.30) without the delta function term,  $C_F$  and  $T_F$  are the Casimir invariants from (2.27), and  $P_{q\bar{q},qg}^{(0)}$  are the DGLAP splitting functions [15, 16, 17] given as

$$P_{q\bar{q}}^{(0)}(z) = \frac{C_F}{2} \left( \frac{3}{2} \delta(1-z) + \frac{2}{(1-z)_+} - (1+z) \right), \quad (3.36)$$

and

$$P_{qg}(z) = \frac{T_F}{2} (z^2 + (1-z)^2). \quad (3.37)$$

Lastly, the SUSY-QCD corrections are given from [20] as

$$\begin{aligned} \frac{d\sigma_{q\bar{q}}^{(1;\text{SUSY})}}{dz} = \frac{\alpha^2 \pi C_F \beta^3}{36M^2} & \left( f_\gamma e_q^2 e_l^2 \delta^{ij} + f_{\gamma Z} \frac{e_q e_l \delta^{ij} \text{Re}[L_{Z\tilde{l}_i\tilde{l}_j} + R_{Z\tilde{l}_i\tilde{l}_j}]}{4\sin^2\theta_W(1-\sin^2\theta_W)(1-m_Z^2/M^2)} \right. \\ & \left. + f_Z \frac{|L_{Z\tilde{l}_i\tilde{l}_j} + R_{Z\tilde{l}_i\tilde{l}_j}|^2}{32\sin^4\theta_W(1-\sin^2\theta_W)^2(1-m_Z^2/M^2)^2} \right) \delta(1-z), \end{aligned} \quad (3.38)$$

where the virtual loop corrections of  $f_\gamma$ ,  $f_{\gamma Z}$  and  $f_Z$  can be found in appendix B of [20].

We can now find the full partonic cross section to next-to-leading order by inserting the corrections we have found into (3.7). This results in

$$\frac{d\hat{\sigma}_{ab}}{dz} = \frac{d\sigma_{q\bar{q}}^0}{dz} + \frac{\alpha_s}{\pi} \left[ \frac{d\sigma_{q\bar{q}}^{(1;\text{QCD})}}{dz} + \frac{d\sigma_{qg}^{(1;\text{QCD})}}{dz} + \frac{d\sigma_{q\bar{q}}^{(1;\text{SUSY})}}{dz} \right], \quad (3.39)$$

where we need to sum over the partons  $a$  and  $b$  before inserting this into the integral over the fractional momenta  $x_a$  and  $x_b$  in (3.5) to get the full cross section for a given slepton mass. This will be done in the next chapter through a numerical evaluation and integration.



# Chapter 4

## Numerical Calculation of Cross Sections

In high energy physics calculations, we often are moved to evaluate the same cross section many times. This is a consequence of trying to fit models to experimental data generated through experiments at for example LHC and Tevatron, where there are numerous free parameters that needs fitting. The cross section will therefore have to be evaluated for all the different parameters to get a good prediction of whether or not the model fits with the data. This is the main reason as to why a faster and improved method at calculating these cross sections numerically is needed, as less time will be spent on searching the parameter space and more time can be spent analysing the data or further improving the model.

The main focus of the computational part of this thesis is to incorporate `VegasFlow` [28] and `PDFFlow` [29] in the cross section calculation in order to get better opportunities for parallelisation on both CPUs and GPUs. This is done so that we can achieve a higher speed up in calculations and then have a better starting point to explore the large parameter space of the MSSM model.

### 4.1 Parton distribution functions

Parton distribution functions (PDFs) are a big bottleneck when it comes to speeding up the process of calculating any proton collision cross section. We can see this by looking at the main function for calculating pair production cross sections given in equation (3.5). In that equation we see that for every point in the phase space integral  $x_a$  and  $x_b$ , we need to estimate a new value for the PDFs in addition to the calculation of the hard partonic  $q\bar{q} \rightarrow \tilde{l}_i\tilde{l}_j^*$  process. Normally this has been done by accessing the LHAPDF [30] library tool to download and make use of global fits to PDF data from different research groups. When a PDF set have been downloaded, it can be used to evaluate the value of  $x f_i(x, \mu_F^2)$  for a given value of  $x$ ,  $\mu_F^2$ , and a specific parton ID,  $i$ , of the process, where  $\mu_F$  is the unphysical factorization scale. These parton IDs

follow from the convention set by the Particle Data Group (PDG) [31] where particles are given positive numbers while anti-particles are negative numbers. The parton IDs that appear in the proton are the quarks and gluon given as  $d, u, s, c, b = 1, 2, 3, 4, 5$ , and  $g = 21$  where the top quark does not contribute to the cross section that we are considering, as it is too heavy.

With the given parton IDs we would have to sum over all the partons that can contribute from the anti-particles and the particles. There is however no difference if parton  $a$  is the particle and parton  $b$  is the anti-particle or vice versa; one can cut the summation in two by instead just summing over the particle IDs and adding a factor of 2 as

$$\sigma = 2 \sum_{a=1}^5 \int dx_a \int dx_{-a} f_i(x_a, \mu_F^2) f_{-i}(x_{-a}, \mu_F^2) \hat{\sigma}_{a,-a}. \quad (4.1)$$

The traditional way of calculating this numerically is through a given PDF set from the LHAPDF library and an integration routine, such as the VEGAS algorithm described in [32]. This is a Monte Carlo based algorithm which leads to the problem discussed above of multiple calls to the LHAPDF library to get the values needed for the PDFs.

We can now note that for each point in the parameter space, the values of the PDFs are independent of the other points. This problem then screams to be parallelised where we can, through a single call to the PDFs, estimate the value of these for multiple  $x$  and  $\mu_F^2$  values at the same time. This is where the PDFFlow and VegasFlow algorithms comes in. These algorithms build upon the open source TensorFlow program where GPU compatibility is built into the tool. With these two algorithms, we can use VegasFlow to generate a tensor array of  $x$  values and corresponding  $\mu_F^2$  values. These values are then taken up by PDFFlow to return the values for  $xf(x, \mu_F^2)$  for each of the elements in the tensor array. This way we only need to call the PDF sets once, and then we have all the needed values in storage to access when the computation of the hard process is done. We can also add an additional tensor array consisting of the particle IDs before summing over this dimension in the tensor matrix of  $xf(x, \mu_F^2)$  so that the summation is done inside of the integration.

The different PDF sets that can be found in the LHAPDF library are often fitted to very different data from many specific experiments such as LHC data and anti proton data. This leads to a lot of consideration of which PDF set is best suited to the calculations done in this thesis. Since we are focusing on proton collisions at the LHC, it is natural for us to use up-to-date PDF sets that have also been fitted to data from the LHC. This is why we use the PDF4LHC15\_nlo\_mc\_pdfas set described in the PDF4LHC article [33] and the newly released PDF4LHC21\_mc\_pdfas set [34] fitted to data from the LHC.

## 4.2 Numerical error calculations

When calculating anything numerically, there are always assumptions made that will lead to numerical uncertainties. In this section we will discuss three of these numerical uncertainties that arise and how to handle them. The first of these errors is the scale factor, the second is the PDF error, and the third is the error in the strong coupling constant.

### 4.2.1 Factorization and renormalization scale error

The factorization scale,  $\mu_F$ , is the scale that is introduced to remove any IR divergences from the hard scattering process. With this, the PDFs becomes a function of this scale. Since this is an unphysical scale, it is often set to be the same as the mass,  $m_{\tilde{l}}$ , of the slepton pair,  $\mu_F^2 = m_{\tilde{l}}^2$ . The renormalization scale,  $\mu_R$ , is the scale used to determine the running of the strong coupling constant  $\alpha_s(\mu_R^2)$  at a given energy scale. This is also an unphysical scale and for simplicity, it is also set to be equal to the slepton mass which is equal to the factorization scale,  $\mu_R^2 = \mu_F^2 = m_{\tilde{l}}^2$ .

By varying these scales, we can notice that the leading order cross section has a slight dependence on the factorization scale, while the next-to-leading order cross section has a dependence on the renormalization scale with the factorization scale. This dependence on the renormalization scale will drop out if we can sum over the whole perturbation series, but that is a practical impossibility. Instead we normally say that the higher order contributions introduces an error where the highest and lowest contribution can be found by setting the scale to be  $2\mu_R$  and  $\mu_R/2$ . We can also find the error from the factorization scale in a similar way by setting the scale to be  $2\mu_F$  and  $\mu_F/2$ . This choice is rather arbitrary, but it gives a good estimate for the error of the renormalization and factorization scale.

### 4.2.2 PDF uncertainties

The PDF sets given by the different research groups are a global fit to data from different particle colliders where the researchers need to do numerous interpolations and estimations to extrapolate the data of the PDFs to any value of  $x$  and  $\mu_F$  one might enter to the function. Because of this, they create several members or replicas to the same PDF set, from which one can compute numerical errors. This is different for each PDF set, and it is described in the article that compliments the set in question.

For our PDF sets, we use the description from chapter 6 in both of the PDF4LHC articles [33, 34]. We use the Monte Carlo set, so we must consider the uncertainty prescription for this sets. The 0th member is given as the central value,  $\langle\sigma\rangle \approx \sigma^{(0)}$ , while the rest,  $\sigma^{(k)}$  can be used to calculate the uncertainties. The first way is to

calculate the standard deviation of the distribution as

$$\delta^{\text{pdf}}\sigma = \sqrt{\frac{1}{N_{\text{mem}} - 1} \sum_{k=1}^{N_{\text{mem}}} (\sigma^{(k)} - \langle\sigma\rangle)^2}, \quad (4.2)$$

where  $N_{\text{mem}} = 100$  in our case.

Another more commonly used method for the Monte Carlo sets is to find the 68% confidence level (CL) of the set which corresponds to  $1\sigma$  of a Gaussian distribution. This is done by first denoting  $\mathcal{F}_k$  as the physical observable computed using the  $k$ -th member of the PDF set. We can then order the observables in ascending order with  $\mathcal{F}_1$  being the smallest and  $\mathcal{F}_{N_{\text{mem}}}$  being the largest. Next we can remove  $(100 - 68)\% = 32\%$  of the replicas with 16% on each side so that we are left with the set  $[\mathcal{F}_{0.16N_{\text{mem}}}, \mathcal{F}_{0.84N_{\text{mem}}}]$ . In our case, with  $N_{\text{mem}} = 100$ , we can then find the uncertainty as the difference between the two extremities of the new set, divided by a factor of 2. The 68% CL PDF uncertainty is then given as

$$\delta^{\text{pdf}}\sigma = \frac{\mathcal{F}_{84} - \mathcal{F}_{16}}{2}. \quad (4.3)$$

With these members, there are regions of greater uncertainties specifically for large  $x$  values, where the observables can be calculated to a negative value for a given member  $k$ . For cross sections however, we know from physical constraints that they need to be positive, so we are required to modify these results. The prescription for doing this when  $\mathcal{F}_k < 0$  for a given replica  $k$  is to simply set  $\mathcal{F}_k = 0$  in these situations.

### 4.2.3 Adding $\alpha_s$ uncertainties

Now with the PDF uncertainties in hand, we can turn to the uncertainties in the strong coupling constant  $\alpha_s$ . This constant is also determined experimentally while fitting the same PDF sets, and the central value for  $\alpha_s$  in the PDF4LHC21 sets are given as

$$\alpha_s(M_Z^2) = 0.1180 \pm 0.0010, \quad (4.4)$$

at the 68% CL, with  $M_Z$ , the mass of the Z-boson, being the renormalization scale used.

The PDF set therefore includes two additional members, where the strong coupling constant is the upper and lower value respectively. With these members one can compute the total PDF+ $\alpha_s$  uncertainty by using the procedure above with the  $\alpha_s$  being the central value, then computing the upper and lower prediction for the two  $\alpha_s$  values. The PDF replicas using the upper and lower prediction for the  $\alpha_s$  values are the two last members of the set,  $k = 101$  and  $k = 102$ . Using these PDF replicas and inserting the new value of  $\alpha_s$  in the cross section, the  $\alpha_s$  uncertainty can be found as

$$\delta^{\alpha_s}\sigma = \frac{\sigma(\alpha_s = 0.119) - \sigma(\alpha_s = 0.117)}{2}, \quad (4.5)$$

where  $\delta^{\alpha_s}\sigma$  are the  $\alpha_s$  uncertainty. This corresponds to an uncertainty of  $\delta\alpha_s = 0.001$  at the 68% CL. After we calculate the two uncertainties, we can add them together according to the prescription mentioned in [35], so that

$$\delta\sigma = \sqrt{(\delta^{\text{pdf}}\sigma)^2 + (\delta^{\alpha_s}\sigma)^2}. \quad (4.6)$$

For the PDF4LHC15 sets, however, the  $\alpha_s$  given here is

$$\alpha_s(M_Z^2) = 0.1180 \pm 0.0015. \quad (4.7)$$

In (4.5) we instead have to use  $\alpha_s(M_Z^2) = 0.1195$  and  $\alpha_s(M_Z^2) = 0.1165$  respectively, but otherwise the procedure is still the same for calculating the  $\alpha_s$  uncertainty and combining with the PDF uncertainty to get the total uncertainty of the cross section.

## 4.3 Results of numerical calculations

We are now ready to calculate the cross sections and uncertainties numerically. For the parameters of the standard model, we use the current values of  $m_W = 80.377$  GeV and  $m_Z = 91.1876$  GeV as the masses of the  $W$  and  $Z$  bosons, and  $G_F = 1.16637 \cdot 10^{-5}$  GeV<sup>-2</sup> as the world average value for the Fermi coupling constant, all taken from the Particle Data Group [36]. We can then use these values to define the other parameters we need, such as the squared sine of the electroweak angle

$$\sin^2\theta_W = 1 - \left(\frac{m_W}{m_Z}\right)^2, \quad (4.8)$$

and the electromagnetic fine structure constant

$$\alpha = \sqrt{2}G_F m_W \sin^2\theta_W / \pi, \quad (4.9)$$

and the electric charge as

$$e = \sqrt{4\alpha\pi}. \quad (4.10)$$

We will also run our calculations at a center of mass energy of  $\sqrt{S} = 13$  TeV which is the same as the energy of the collisions in LHC's  $pp$ -collider. Here,  $S$  is used as the proton center-of-mass energy so that the partonic center-of-mass energy becomes  $s = x_a x_b S$ .

We can now start to generate results, and firstly we wanted to check the PDFFlow package by generating results for  $x f_q(x, Q^2)$  for a given  $Q^2$  for both the PDF4LHC15 and PDF4LHC21 sets. These results are shown in figure 4.1 and 4.2. Here we cannot see any major differences in the two PDF sets. For a more detailed description of the sets see [33] and [34].



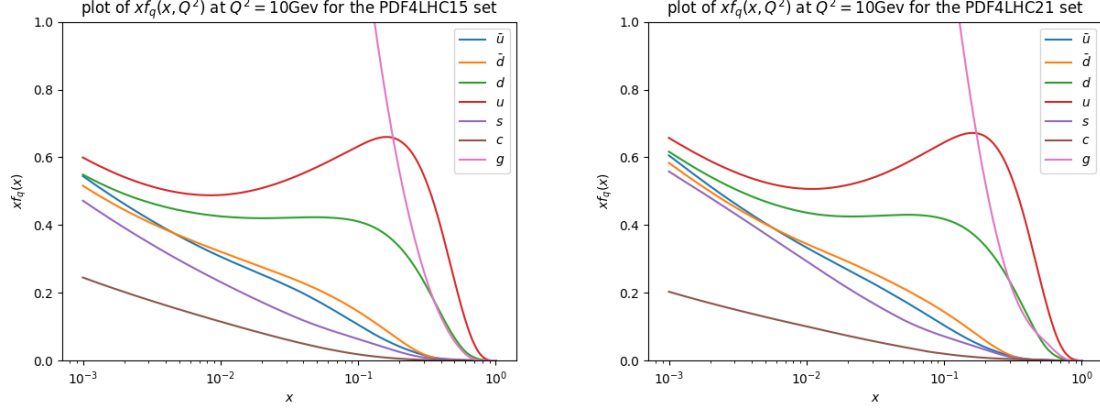


Figure 4.1: Results for  $xf_q(x, Q^2)$  for both the PDF4LHC15 and the PDF4LHC21 sets with  $Q^2 = 10$  GeV and  $q = u, d, s, c, \bar{u}, \bar{d}, g$ .

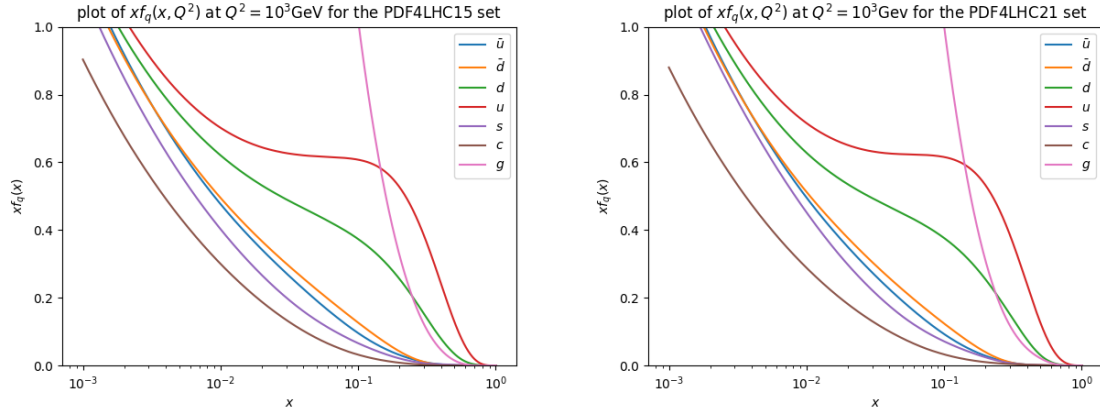


Figure 4.2: Results for  $xf_q(x, Q^2)$  for both the PDF4LHC15 and the PDF4LHC21 sets with  $Q^2 = 10^3$  GeV and  $q = u, d, s, c, \bar{u}, \bar{d}, g$ .

After confirming the usage of the parton distribution functions, we can numerically evaluate the equation (3.5) from the partonic leading- and next-to-leading order contributions found in chapter 3. Then we can study the cross section dependence on the mass of the slepton pair and showcase the different uncertainties that we have calculated. Firstly, we have the scale dependence where we vary the scale  $\mu_F, \mu_R$  to the minimal and maximal values of  $m_{\tilde{l}}/2$  to  $2m_{\tilde{l}}$ . This is shown in the figures 4.3 and 4.4. Then we explicitly show the mass dependence of  $\tilde{e}_L \tilde{e}_L^*$  and  $\tilde{e}_R \tilde{e}_R^*$ . Additionally we will also show both the PDF uncertainties and  $\alpha_s$  uncertainties of the selectron cross section. This will be done both separately and added together according to (4.6).

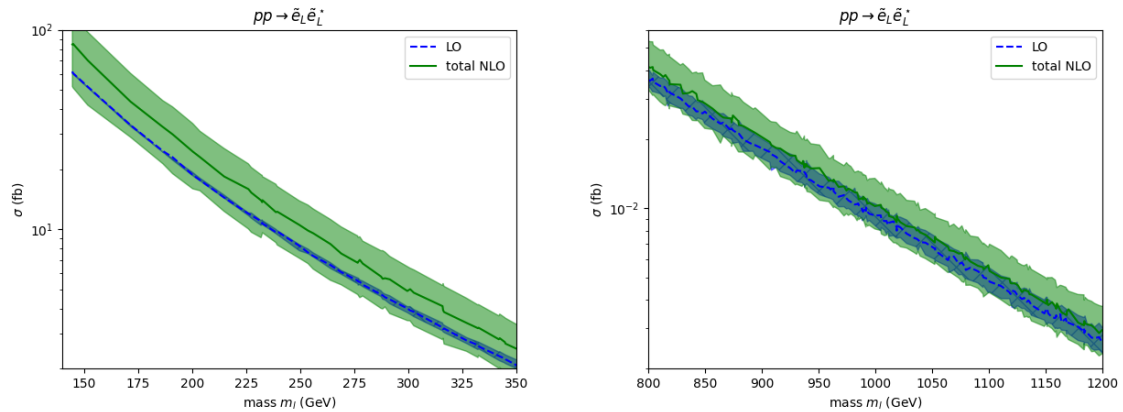


Figure 4.3: The mass dependence of the left handed selectron cross section together with the scale uncertainties where  $\mu_F = \mu_R = 2m_{\tilde{l}}$  and  $\mu_F = \mu_R = m_{\tilde{l}}/2$ . These are calculated with the PDF4LHC15 set.

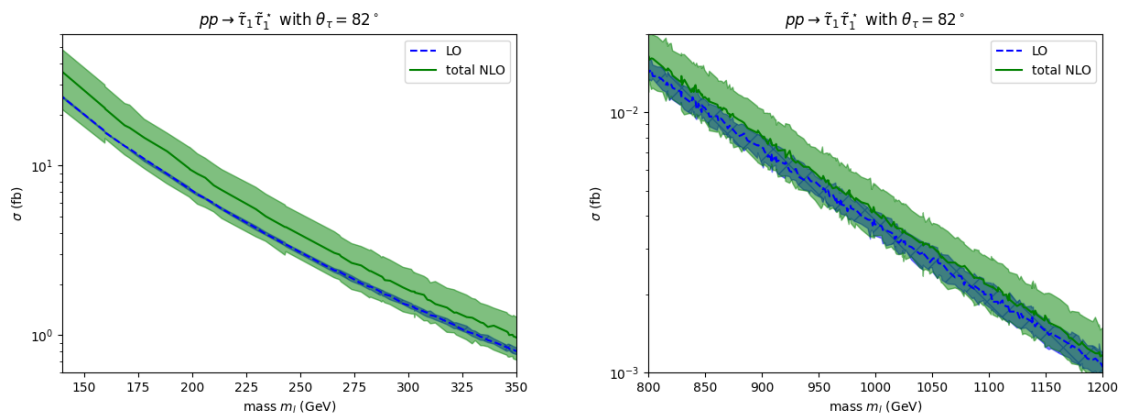


Figure 4.4: The mass dependence of the stau<sub>1</sub> cross section together with the scale uncertainties where  $\mu_F = \mu_R = 2m_{\tilde{l}}$  and  $\mu_F = \mu_R = m_{\tilde{l}}/2$ . These are calculated with the PDF4LHC15 set.

The above figures show the scale uncertainties of the leading order and the next-to-leading order cross sections. We have included both the left handed selectron pair production and the stau pair production. From the graphs, we can notice how the relative scale uncertainty increases as the mass of the slepton pair also increases. Additionally, the leading order contribution only picks up a factorization scale uncertainty as this result is independent of the factorization scale,  $\mu_R$ .

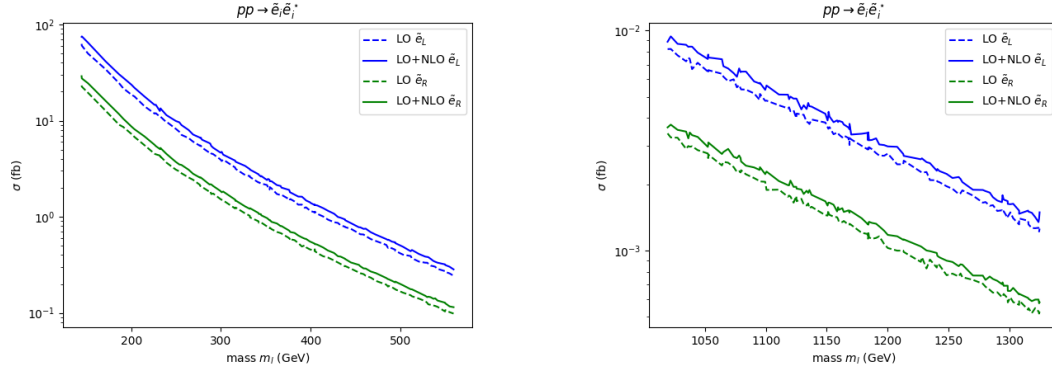


Figure 4.5: The mass dependence of the selectron cross section for both the production of the left handed and the right handed mass eigenstate.

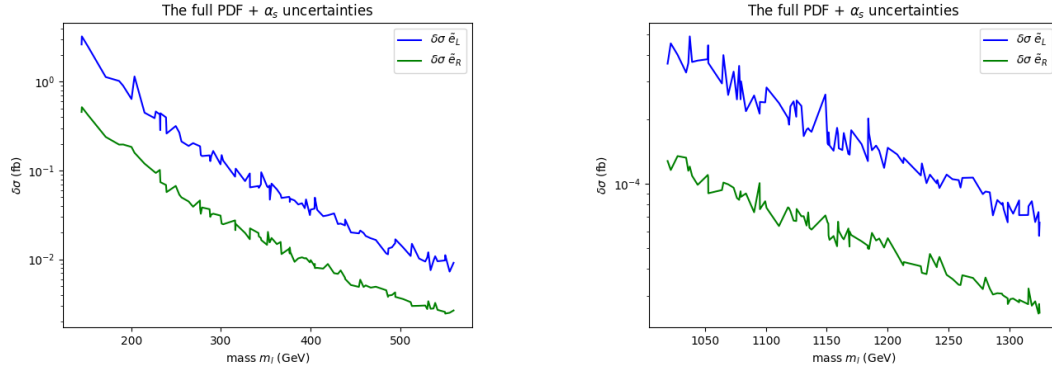


Figure 4.6: This figure shows the full calculated PDF+\$\alpha\_s\$ uncertainties for both the production of the left handed and the right handed mass eigenstate.

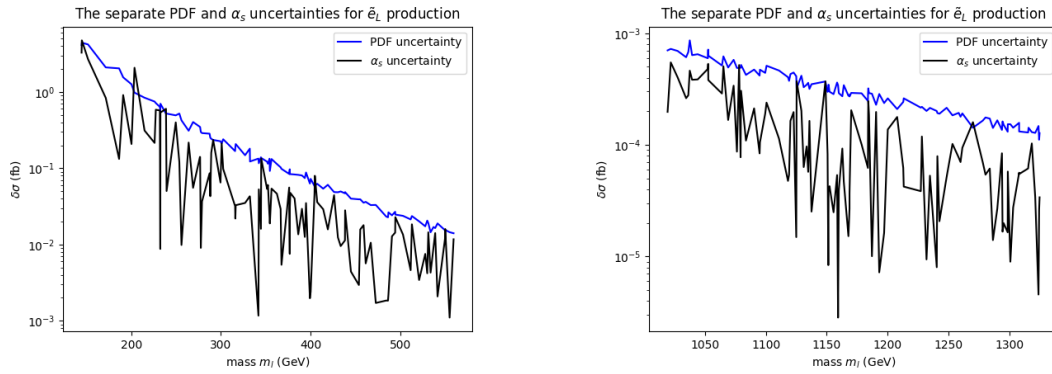


Figure 4.7: Here we have visualised calculated PDF and \$\alpha\_s\$ uncertainties separately for the production of the left handed selectron.

The figures 4.5, 4.6 and 4.7 shown above have all been calculated using the PDF4LHC15 sets. The figures on the left side represent low slepton masses while the figures on the right represent higher slepton masses. We can then notice from these that the uncertainties are about an order of magnitude smaller than the cross section calculated. In addition, the PDF uncertainties that was evaluated from 100 different replicas of the PDF set are much more even than the  $\alpha_s$  uncertainties

In figure 4.8 we have calculated the relative difference of left-handed selectron pair production at leading order and next-to-leading order of our calculations against the same calculations using PROSPINO [37]. In the NLO contribution, one can note a slight shift in the results; this is due to us being unable to calculate the SUSY virtual loop coefficients,  $f_\gamma, f_{\gamma, Z^0}, f_{Z^0}$ . These calculations are normally done through the module LoopTools [38]. We had difficulties installing this library and making it into a dynamic style library for sharing between Python and C++, so we have therefore decided to omit this calculation from the rest of the results. However, since the calculations of the PDFs is a big bottleneck in numerically evaluating cross sections, we believe we can still consider speed up at this level of the calculations without the SUSY contributions. Any extra time needed to calculate the SUSY contributions would be the same whether or not we include the PDFFlow and VegasFlow modules.

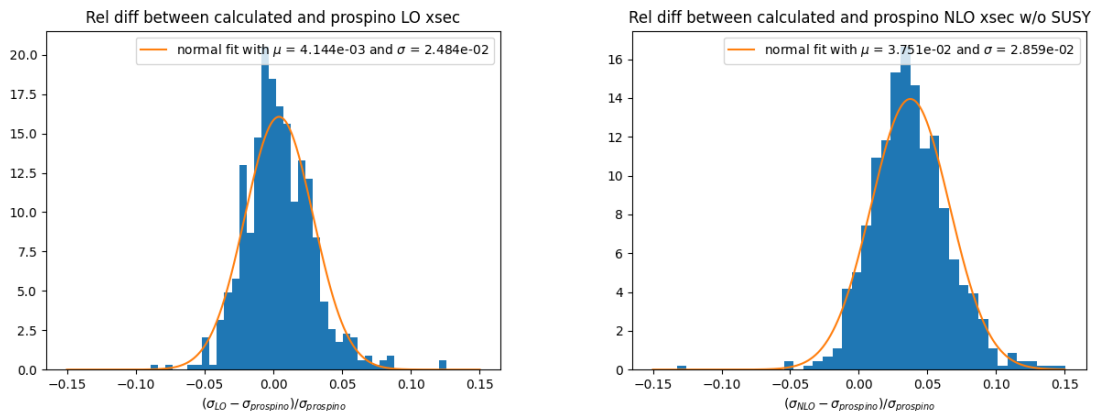


Figure 4.8: The relative difference between our calculations of the left handed selectron pair production against the same calculations from PROSPINO

Finally, we want to look at the time taken to calculate these parton distribution functions. For the full calculation of both PDF uncertainties and  $\alpha_s$  uncertainties, we will have to calculate the same cross section 103 times in total, once to get the standard value from member zero, then 100 times in order to generate the full PDF uncertainty, and lastly two more times to get the  $\alpha_s$  uncertainty. In figure 4.9 we show the time taken for each new member of the PDFs that we calculate until we have finished with all 103 members. The orange line represents the calculation of the cross section without the use of modules, while the blue line represents the use of PDFFlow

and `VegasFlow` where you initialize one PDF set at a time. Comparing these lines, we see that the use of `PDFFlow` and `VegasFlow` almost halves the time spent. In total, we found that calculating all the uncertainties for a single point in the parameter space takes around 156.4 seconds. The green line still represents use of the above modules but instead with the initialization of ten PDF sets at a time for the PDF members between [1, 100]. Comparing the green line to the results from initializing just one PDF at a time, we notice that the heavy load of downloading and computing  $xf_q(x, Q^2)$  for each calculation significantly increases the time spent calculating. This has the potential of being even more efficient if one can use `VegasFlow` to integrate over all the ten cross sections at the same time, either through some sort of parallelization or vectorization.

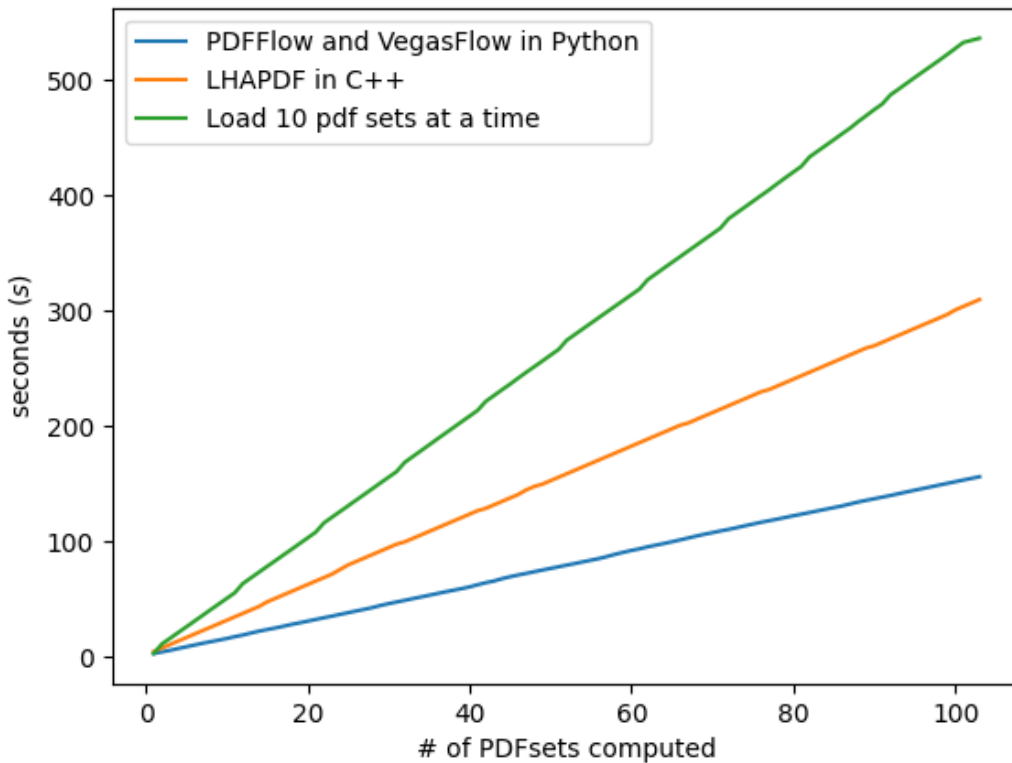


Figure 4.9: Time comparison between using `PDFFlow` and `VegasFlow` in Python against the classical way of calculating PDFs through `Lhapdf` in C++.



# Conclusion

The goal of this thesis was to use `PDFFlow` and `VegasFlow` in `Python` to numerically evaluate cross sections in a way that sped up the calculations compared to the standard way of calculating these cross sections through the use of `LHAPDF` in `C++`. We have then investigated the construction of the quantum field theory, which led us to be able to calculate the slepton pair production to leading order. We then explored the uncertainties and the mass dependence of this cross section before looking at the amount of time a single point in parameter space took to completely evaluate with uncertainties.

In order to achieve our results, we first looked at how gauge theories are constructed in chapter 1. In this chapter we discussed Lie groups and how they could be used to create invariant Lagrangians under symmetries of the given group. We then used these Lagrangians together with the path integral formalism to derive the Feynman rules of quantum field theory for the  $SU(N)$  symmetry group. Next, we considered in chapter 2 the evolution of the deep inelastic scattering from the classical Coulomb scattering result. The results of higher energy experiment of this scattering showed point like constituents that Feynman called partons, and he introduced them in his parton model. With this model one can predict a theoretical independence on the energy  $Q^2$  for a given Bjorken  $x$ . Then, when introducing QCD as an  $SU(3)$  symmetry group, we can confirm Bjorken scaling to leading order and at the same time find the next-to-leading order corrections which showed there was a weak logarithmic dependence on  $Q^2$ .

For chapter 3, we turned to new beyond the standard model physics. One of the many theories that tries to explain phenomenons such as dark matter and dark energy is the theory of supersymmetry. Here, we gave a brief overview of this theory while listing up the standard model particles and their supersymmetric partner in the minimal supersymmetric standard model. We then listed up a couple of Feynman rules for the sleptons which we needed to calculate the leading order contribution to slepton pair production. The interaction was then mediated by either a photon or a  $Z^0$ -boson. With this we resulted with three terms in the interaction matrix element which included the squared photon and  $Z^0$  contribution, and the photon,  $Z^0$  interference term. Finally, we cited the next to leading order results from [20].

In chapter 4, we discussed how to numerically evaluate the cross sections and how to deal with uncertainties. We noticed that dealing with parton distribution functions has always been a big bottleneck in computations. In this thesis we made use of the program `PDFFlow` which is a python `TensorFlow` module wrapped around the `LHAPDF` library. We then considered the uncertainties that arise from the unphysical scale factors, the PDF uncertainties and the  $\alpha_s$  uncertainties. In the end, we discussed the different results we found from our calculations such as the time decrease found from the use of both of the `TensorFlow` modules.

Further considerations from this thesis would be to work with the numerically evaluations in order to parameterize the code such that the amount of time one saves

for each point in parameter space is increased. We should also continue with working on GPUs so that we can fully take advantage of the TensorFlow background of the two modules we used.



# Appendix A

## Code repository

The code used in this thesis will be publically available along with the data used in the Github repository of <https://github.com/martimc/MasterWork>. Here the `Full_xsec.cpp` program calculates the leading order and next-to-leading order contribution in C++ without the use of the `VegasFlow` or `PDFFlow` modules

The `func_lib` programs generates the shared library as a `.so` file for Ubuntu/LINUX while the `.dylib` file is used for mac compilations. Then we can make use of the above modules in Python which has been implemented in the `Xsec_calc.py` file. This program is called by

```
$ python3 Xsec_calc.py 'input_file' 'output_file' 'slepton_pair_code'
```

As an example one could write

```
$ python3 Xsec_calc.py 'sleptons_MSSM24.dat' 'selectrons_out.dat'  
'100011_-100011'
```

to get the values of left-handed selectron pair production given in the file `selectrons_out.dat`

The main calculation part of `Xsec_calc.py` is done in the function

```
def NLO_integrand(xarr, n_dim = None, weight = None):  
    M2 = xarr[:,1]*xarr[:,2]*struct.S  
    z = xarr[:,0]  
    n = len(z.numpy())  
    struct.M2 = npct.as_ctypes(M2.numpy())  
    struct.z = npct.as_ctypes(z.numpy())  
  
    q2 = tf.fill(tf.shape(xarr[:,0]), struct.mu_F**2)  
    q2 = tf.cast(q2, tf.float64)  
    pid = tf.cast([1,2,3,4,5], dtype=tf.int32)  
    pid_g = tf.cast([21], dtype=tf.int32)  
    pid_rev = -1*pid  
  
    pid_array = pid.numpy()
```

```

struct.pid = npct.as_ctypes(pid_array)
imem = struct.PDF_mem

if (0<imem and imem < 101):
    pdfs_a = pdf.xfxQ2(pid, xarr[:,1], q2)[imem-1]
    pdfs_b = pdf.xfxQ2(pid_rev, xarr[:,2], q2)[imem-1]
    pdfs_g = pdf.xfxQ2(pid_g, xarr[:,2], q2)[imem-1]

else:
    pdfs_a = pdf.xfxQ2(pid, xarr[:,1], q2)
    pdfs_b = pdf.xfxQ2(pid_rev, xarr[:,2], q2)
    pdfs_g = pdf.xfxQ2(pid_g, xarr[:,2], q2)

if imem == 101:
    alpha_s = pdf.alphasQ2(q2)-0.0015
elif imem == 102:
    alpha_s = pdf.alphasQ2(q2)+0.0015
else:
    alpha_s = pdf.alphasQ2(q2)

struct.alpha_s = npct.as_ctypes(alpha_s.numpy())

struct_pointer = ctypes.byref(struct)

struct.n = ctypes.c_int(n)
Z1_xsec = np.zeros(struct.n*5)
LO_xsec = np.zeros(struct.n*5)
struct.Z1_xsec = npct.as_ctypes(Z1_xsec)
struct.LO_xsec = npct.as_ctypes(LO_xsec)

c_lib.LO_cross(struct_pointer)
c_lib.Z1_cross(struct_pointer)

vec_LO_xsec = tf.cast(LO_xsec, tf.float64)
tf_LO_xsec = tf.reshape(vec_LO_xsec, shape=(n, 5))

vec_Z1_xsec = tf.cast(Z1_xsec, tf.float64)
tf_Z1_xsec = tf.reshape(vec_Z1_xsec, shape=(n, 5))

C_F = 4.0/3
T_R = 1.0/2
z2 = tf.math.square(z)
ones = tf.ones(M2.shape, dtype=tf.float64)

```

```

qq_term1 = -1 * (ones + z2) / (ones - z) * tf.math.log(z)
qq_term2 = -2 * (ones + z) * tf.math.log(ones - z)
qq_term3 = -1 * (ones + z) * tf.math.log(M2 / struct.mu_F**2)

qg_terms = (ones / 2 - z + z2) * tf.math.log(tf.math.square(ones - z)\
/ z) + ones / 4 + 3 * z / 2 - 7 * z2 / 4\
+ P_qg(z, T_R) / T_R * tf.math.log(M2 / (struct.mu_F**2))

xsec_Z1 = 2*tf.reduce_sum((tf_Z1_xsec*pdfs_a*pdfs_b), axis = 1)\
/(xarr[:,1]*xarr[:,2])

qq_term = 2*tf.reduce_sum((tf_LO_xsec*pdfs_a*pdfs_b), axis = 1)\
*alpha_s*C_F/(np.pi*xarr[:,1]*xarr[:,2])*(qq_term1+qq_term2+qq_term3)

qg_term = 2 * (tf.reduce_sum((tf_LO_xsec*pdfs_a), axis = 1)\
+tf.reduce_sum((tf_LO_xsec*pdfs_b), axis = 1))\
*pdfs_g*alpha_s*T_R/(np.pi*xarr[:,1]*xarr[:,2])*qg_terms

NLO_res = xsec_Z1 + qq_term + qg_term
return NLO_res

```

where the functions `c_lib.L0_cross()` and `c_lib.Z1_cross()` calls these functions from the `func_lib` library.

# Bibliography

- [1] M.E. Peskin and D.V. Schroeder, *An Introduction to quantum field theory*, Addison-Wesley, Reading, USA (1995).
- [2] M.D. Schwartz, *Quantum Field Theory and the Standard Model*, Cambridge University Press (3, 2014).
- [3] M. Gell-Mann, *Symmetries of baryons and mesons*, *Phys. Rev.* **125** (1962) 1067.
- [4] J.E. Kim and H.P. Nilles, *The mu Problem and the Strong CP Problem*, *Phys. Lett. B* **138** (1984) 150.
- [5] L.D. Faddeev and V.N. Popov, *Feynman Diagrams for the Yang-Mills Field*, *Phys. Lett. B* **25** (1967) 29.
- [6] P.W. Higgs, *Broken Symmetries and the Masses of Gauge Bosons*, *Phys. Rev. Lett.* **13** (1964) 508.
- [7] F. Englert and R. Brout, *Broken Symmetry and the Mass of Gauge Vector Mesons*, *Phys. Rev. Lett.* **13** (1964) 321.
- [8] R.P. Feynman, *The behavior of hadron collisions at extreme energies*, *Conf. Proc. C* **690905** (1969) 237.
- [9] J.C. Ward, *An Identity in Quantum Electrodynamics*, *Phys. Rev.* **78** (1950) 182.
- [10] W. Albrecht, H.J. Behrend, F.W. Brasse, W. Flauger, H. Hultschig and K.G. Steffen, *Elastic electron-proton scattering at momentum transfers up to  $245 \text{ f}^{-2}$* , *Phys. Rev. Lett.* **17** (1966) 1192.
- [11] J.D. Bjorken, *Asymptotic Sum Rules at Infinite Momentum*, *Phys. Rev.* **179** (1969) 1547.
- [12] C.G. Callan, Jr. and D.J. Gross, *High-energy electroproduction and the constitution of the electric current*, *Phys. Rev. Lett.* **22** (1969) 156.
- [13] PARTICLE DATA GROUP collaboration, *Review of Particle Physics (RPP)*, *Phys. Rev. D* **86** (2012) 010001.

- [14] G. Altarelli, R.K. Ellis, G. Martinelli and S.-Y. Pi, *Processes Involving Fragmentation Functions Beyond the Leading Order in QCD*, *Nucl. Phys. B* **160** (1979) 301.
- [15] Y.L. Dokshitzer, *Calculation of the Structure Functions for Deep Inelastic Scattering and  $e^+ e^-$  Annihilation by Perturbation Theory in Quantum Chromodynamics.*, *Sov. Phys. JETP* **46** (1977) 641.
- [16] V.N. Gribov and L.N. Lipatov, *Deep inelastic  $e p$  scattering in perturbation theory*, *Sov. J. Nucl. Phys.* **15** (1972) 438.
- [17] G. Altarelli and G. Parisi, *Asymptotic Freedom in Parton Language*, *Nucl. Phys. B* **126** (1977) 298.
- [18] J.C. Collins, D.E. Soper and G.F. Sterman, *Factorization of Hard Processes in QCD*, *Adv. Ser. Direct. High Energy Phys.* **5** (1989) 1 [[hep-ph/0409313](#)].
- [19] R.G. Newton, *Optical theorem and beyond*, *American Journal of Physics* **44** (1976) 639.
- [20] G. Bozzi, B. Fuks and M. Klasen, *Threshold Resummation for Slepton-Pair Production at Hadron Colliders*, *Nucl. Phys. B* **777** (2007) 157 [[hep-ph/0701202](#)].
- [21] Y.A. Gol'Fand and E.P. Likhtman, *Extension of the Algebra of Poincare Group Generators and Violation of  $P$  invariance*, *Soviet Journal of Experimental and Theoretical Physics Letters* **13** (1971) 323.
- [22] H. Murayama, *Supersymmetry phenomenology*, in *ICTP Summer School in Particle Physics*, pp. 296–335, 2, 2000 [[hep-ph/0002232](#)].
- [23] S. Weinberg, *A Model of Leptons*, *Phys. Rev. Lett.* **19** (1967) 1264.
- [24] MSSM WORKING GROUP collaboration, *The Minimal supersymmetric standard model: Group summary report*, in *GDR (Groupement De Recherche) - Supersymetrie*, 12, 1998 [[hep-ph/9901246](#)].
- [25] J. Rosiek, *Complete set of Feynman rules for the MSSM: Erratum*, [hep-ph/9511250](#).
- [26] P. Richardson, *Simulations of  $R$ -parity Violating SUSY Models*, Ph.D. thesis, Oxford U., 2000. [hep-ph/0101105](#).
- [27] S. Mandelstam, *Determination of the pion - nucleon scattering amplitude from dispersion relations and unitarity. General theory*, *Phys. Rev.* **112** (1958) 1344.

- [28] S. Carrazza and J.M. Cruz-Martinez, *VegasFlow: accelerating Monte Carlo simulation across multiple hardware platforms*, *Comput. Phys. Commun.* **254** (2020) 107376 [[2002.12921](#)].
- [29] S. Carrazza, J.M. Cruz-Martinez and M. Rossi, *PDFFlow: parton distribution functions on GPU*, [2009.06635](#).
- [30] A. Buckley, J. Ferrando, S. Lloyd, K. Nordström, B. Page, M. Rüfenacht et al., *LHAPDF6: parton density access in the LHC precision era*, *Eur. Phys. J. C* **75** (2015) 132 [[1412.7420](#)].
- [31] L. Garren, I.G. Knowles, T. Sjostrand and T.G. Trippe, *Monte Carlo particle numbering scheme: in Review of Particle Physics (RPP 2000)*, *Eur. Phys. J. C* **15** (2000) 205.
- [32] G.P. Lepage, *VEGAS - an adaptive multi-dimensional integration program*, Tech. Rep. , Cornell Univ. Lab. Nucl. Stud., Ithaca, NY (Mar, 1980).
- [33] J. Butterworth et al., *PDF4LHC recommendations for LHC Run II*, *J. Phys. G* **43** (2016) 023001 [[1510.03865](#)].
- [34] R.D. Ball et al., *The PDF4LHC21 combination of global PDF fits for the LHC Run III*, [2203.05506](#).
- [35] H.-L. Lai, J. Huston, Z. Li, P. Nadolsky, J. Pumplin, D. Stump et al., *Uncertainty induced by QCD coupling in the CTEQ global analysis of parton distributions*, *Phys. Rev. D* **82** (2010) 054021 [[1004.4624](#)].
- [36] E. Tiesinga, P.J. Mohr, D.B. Newell and B.N. Taylor, *CODATA recommended values of the fundamental physical constants: 2018\**, *Rev. Mod. Phys.* **93** (2021) 025010.
- [37] W. Beenakker, R. Hopker and M. Spira, *PROSPINO: A Program for the production of supersymmetric particles in next-to-leading order QCD*, [hep-ph/9611232](#).
- [38] T. Hahn and M. Perez-Victoria, *Automatized one loop calculations in four-dimensions and D-dimensions*, *Comput. Phys. Commun.* **118** (1999) 153 [[hep-ph/9807565](#)].